Geochemistry, Geophysics, Geosystems

RESEARCH ARTICLE
10.1029/2024GC012057

Special Collection:
A fresh look at the Caribbean plate geosystems

Tracking the Caribbean Magmatic Evolution: The British Virgin Islands as a Transition Between the Greater and Lesser Antilles Arcs

Noémie Bosc[1], Delphine Bosch[1], Mélanie Noury[2], Olivier Bruguier[1], Lény Montheil[1], Douwe J. J. van Hinsbergen[3], Jean-Jacques Cornée[1], Jonathan Outin[1], and Mélody Philippon[1]

[1]Géosciences Montpellier, Université de Montpellier, Université des Antilles, CNRS, UMR 5243, Montpellier Cedex, France, [2]Estación Regional del Noroeste, Laboratorio Nacional de Geoquímica y Mineralogía (LANGEM), Instituto de Geología, Universidad Nacional Autónoma de México, Hermosillo, Mexico, [3]Department of Earth Sciences, Utrecht University, Utrecht, The Netherlands

Key Points:

- Magmatism in the British Virgin Islands (BVI) lasted ca. 13 Myrs, from 43 to 30 Ma, along a NE-SW younging trend
- BVI magmatism shows temporal and geochemical similarities with the Greater and Lesser Antilles arcs supporting a shared Eo-Oligocene history
- The BVI are interpreted as delineating a continuous transition between the magmatic systems of the Greater and the Lesser Antilles arcs

Supporting Information:

Supporting Information may be found in the online version of this article.

Correspondence to:

N. Bosc,
noemie.bosc@umontpellier.fr

Citation:

Bosc, N., Bosch, D., Noury, M., Bruguier, O., Montheil, L., van Hinsbergen, D. J. J., et al. (2025). Tracking the Caribbean magmatic evolution: The British Virgin Islands as a transition between the Greater and Lesser Antilles arcs. *Geochemistry, Geophysics, Geosystems*, *26*, e2024GC012057. https://doi.org/10.1029/2024GC012057

Received 11 DEC 2024
Accepted 10 JUN 2025

Author Contributions:

Conceptualization: Noémie Bosc, Delphine Bosch, Mélody Philippon
Data curation: Delphine Bosch, Mélanie Noury, Olivier Bruguier

Abstract

The British Virgin Islands (BVI) archipelago, located between the Greater Antilles and the Lesser Antilles, is a key location to study the geodynamic evolution of the Caribbean plate. Geochemistry of the studied samples reveals typical volcanic arc signatures, including a calc-alkaline affinity, strong negative HFSE anomalies, and LILE enrichment. The εHf values are homogeneous, indicative of a MORB-type mantle. Magmas were sourced from a homogeneous mantle wedge with less than 2% slab-derived sediment inputs, dominated by aqueous fluids. A concomitant melt component has been detected in the Peter and Norman Islands. U-Pb dating emphasizes an active magmatic period spanning over ca. 13 Myr (43–30 Ma), with a NE/SW decreasing age gradient. Thermobarometry data display a SW increasing emplacement depth from ~6 to 13 km. Compared to the Greater and Lesser Antilles, this archipelago shows strong similarities with the extinct northern Lesser Antilles arc in terms of source and age. A geodynamical evolution model is proposed in which this archipelago represents a transition between the Greater and the Lesser Antilles arcs. The Oligocene cessation of magmatism (ca. 30 Ma) may coincide with a regionally documented lull in arc magmatic activity during which the Bahamas bank collided to the north. Paleomagnetic evidence of forearc sliver motion along the northeastern boundary of the Caribbean indicates a northward translation of the archipelago from a position above the Lesser Antilles subduction zone to its modern location along the highly oblique, strike-slip-dominated plate boundary, thus preventing the re-establishment of arc magmatism in the eastern Caribbean.

Plain Language Summary

The Antilles archipelago is a 3,000 km-long volcanic arc located in the Caribbean Sea. It is notable for its longevity, active for over 140 million years, from the Greater Antilles to the Lesser Antilles, and for its complexity, providing valuable insights on the dynamics of island arcs and plate tectonics. The British Virgin Islands, located in an intermediate position between the Greater Antilles to the North and the Lesser Antilles to the South, represent a key strategic point to understand the geodynamic evolution of the Caribbean arc. Fifteen samples from seven British Virgin archipelago islands were studied along the main NE-SW alignment. Geochronological analyses give crystallization ages spanning on 13 Ma and ranging from 43 to 30 Ma. Crystallization depths ranged from 6 to 13 km progressing from NE to SW. Geochemical results, including radiogenic isotopes, indicate strong similarities with the extinct arc of the northern Lesser Antilles, both in terms of recorded processes and magma sources. Taken together, these new results support the idea that the British Virgin Islands represent a transition in the history of the Antilles arc, which starts from the Greater Antilles and continues until present in the Lesser Antilles.

1. Introduction

Along intra-oceanic subduction zones, magmatism is frequently the only geological indicator for studying geodynamics, as most of the upper plates are submerged (e.g., McCulloch & Gamble, 1991). The Antilles arc, sensus lato, is one of the longest-lived intra-oceanic magmatic arc systems that is still associated with active subduction. It thus represents an ideal study area to understand the dynamics and evolution of arc magmatism. Indeed, along nearly all its boundaries, the predominantly oceanic Caribbean plate has been above subduction zones since the Mesozoic. The resulting composite intra-oceanic arc stretches over 3,000 km from the Gulf of Mexico to Venezuela and consists of two main segments. To the north, the Cretaceous to Eocene Greater Antilles arc developed above a southwestward dipping subduction zone that ended with ophiolite emplacement (or arc-

Geochemistry, Geophysics, Geosystems

10.1029/2024GC012057

Formal analysis: Noémie Bosc, Delphine Bosch, Mélanie Noury, Jonathan Outin
Funding acquisition: Delphine Bosch, Mélody Philippon
Investigation: Delphine Bosch, Olivier Bruguier, Mélody Philippon
Methodology: Delphine Bosch, Mélanie Noury, Olivier Bruguier, Jonathan Outin
Project administration: Delphine Bosch, Mélody Philippon
Resources: Delphine Bosch, Mélanie Noury, Mélody Philippon
Supervision: Delphine Bosch, Mélody Philippon
Validation: Delphine Bosch, Mélody Philippon
Visualization: Noémie Bosc, Delphine Bosch, Mélody Philippon
Writing – original draft: Noémie Bosc, Delphine Bosch, Mélanie Noury, Olivier Bruguier, Lény Montheil, Douwe J. J. van Hinsbergen, Jean-Jacques Cornée, Mélody Philippon
Writing – review & editing: Noémie Bosc, Delphine Bosch, Mélanie Noury, Olivier Bruguier, Lény Montheil, Douwe J. J. van Hinsbergen, Jean-Jacques Cornée, Mélody Philippon

continent collision) onto the North American margin (Burke, 1988; Hastie, 2009; Hu et al., 2022; Kerr et al., 1999; Torró et al., 2017). The Greater Antilles arc encompasses the islands of Cuba, Hispaniola, Jamaica, Puerto Rico and the Virgin Islands (Figures 1a and 1b). To the east, the Lesser Antilles arc developed above a westward-dipping subduction zone since the Eocene (Bosch et al., 2022; Carpentier et al., 2008; Davidson, 1987; Labanieh et al., 2010; White & Dupré, 1986) following a change in North and South American and Caribbean relative plate motion (e.g., Boschman et al., 2014; Pindell & Kennan, 2009) (Figure 1a).

The British Virgin Islands (BVI), a NE-SW trending archipelago, expose the easternmost limit of the Greater Antilles arc, and stand at the northern limit of the Lesser Antilles arc (Smith et al., 1998; Wilson et al., 2019) (Figure 1). It comprises a series of Cenozoic igneous rocks intruding metamorphosed volcano-sedimentary Cretaceous series and contains some of the deepest exhumed portions of Caribbean arcs (Jolly & Lidiak, 2006). While there are numerous studies presenting geochemical data on the Greater Antilles (e.g., Härtel et al., 2024; Hastie, 2009; Hu et al., 2022; Kerr et al., 1999; Torró et al., 2017) and Lesser Antilles (e.g., Bosch et al., 2022; Carpentier et al., 2008; Davidson, 1987; Labanieh et al., 2010; White & Dupré, 1986), few studies have been carried out on the BVI (Cox et al., 1977; Jolly & Lidiak, 2006; Kesler & Sutter, 1979; Longshore, 1965; Román et al., 2021; Schrecengost, 2010; Vila et al., 1986). The few ages available for the BVI range from ca. 43 to 24 Ma (see compilation by Hu et al., 2022). Determining whether the transition between the Greater and Lesser Antilles arcs was continuous or happened with a gap in magmatism would give insights into the geodynamic evolution of the region. This question remains debated partly due to geochronologic and geochemical data gaps on the Eastern Caribbean islands, especially the BVI. The present work focuses on the study of magmatic rocks from seven of the BVI, listed from northeast to southwest: Necker (NE), Virgin Gorda (VG), Fallen Jerusalem (FJ), Copper (CO), Salt (SA), Peter (PE), and Norman (NO) (Figure 1c). The main objective of this study is to constrain the evolution of the northeastern corner of the Caribbean plate to better understand the transition between the Greater and the Lesser Antilles arcs. To reach this goal, a petrological, geochemical (major and trace elements, Pb, Sr, Nd, and Hf isotopes), thermobarometric (Al-in-hornblende) and geochronological (U-Pb on accessory minerals) study was carried out. The results are discussed in terms of the nature of the studied rocks, the mantle sources involved and the sediment contributions. The BVI are placed into recent regional geodynamical reconstructions of the NE Caribbean tectonic history in order to interpret these new data in the context of the evolution of the Greater and Lesser Antilles arcs. This allows to highlight correlations and to integrate these new results in recent insights on the Cenozoic northeastern Caribbean tectonic and geodynamic evolution.

2. Geological Setting

The Caribbean Plate is bounded by four other plates (Figure 1a). To the west, the Cocos and Nazca plates subduct beneath the Caribbean and South America plates at a rate of 7 cm/yr (DeMets et al., 2000). To the south, the Caribbean Plate is bounded by the dextral El Pilar—San Sebastian right-lateral transform fault and its related fault systems on- and off-shore that accommodate eastward motion of the Caribbean Plate relative to South America (Audemard, 2009; Colmenares & Zoback, 2003). To the east, the oceanic crust of the North and South American plates subducts beneath the Caribbean plate and the associated Lesser Antilles arc (Macdonald et al., 2000) at a rate of 2 cm/yr (DeMets et al., 2000). This subduction is trench-perpendicular at the latitude of 16°N and subduction obliquity increases northward to reach 77° along the Puerto Rico Trough (Philippon & Corti, 2016). From there, it connects with a sinistral strike-slip system along the northern boundary of the Caribbean plate. This margin, known as the North Caribbean corridor, consists of the Septentrional-Oriente fault to the north and the Anegada, Muertos, Enriquillo Plantain Garden and Swan-Walton faults to the south. Together, these faults delineate a sliver plate located between the North American and the Caribbean plates (Byrne et al., 1985) (Figure 1a). Most of the Caribbean plate interior consists of Mesozoic oceanic crust that formed during the Jurassic, overlain by the Cretaceous Caribbean Large Igneous Plateau (CLIP). The CLIP was emplaced while the plate was part of the Farallon plate and dipping eastward below the Proto-Caribbean Ocean. Since the Cretaceous, the Caribbean plate individualized and moved northeastward between the Americas until the Eocene (Boschman et al., 2014, 2019; Burke, 1988; Pindell & Dewey, 1982; Pindell & Kennan, 2009). From the Eocene onward, two major events occurred: (a) a plate motion reorganization with a switch from northeastward to eastward motion of the Caribbean plate, and (b) arc-continent collision when the Bahamas Bank entered the subduction zone along the northern boundary of the plate (Bralower & Iturralde-Vinent, 1997; Gordon et al., 1997). Consequently, subduction along the Great arc sutured and was reinitiated along the eastern margin of the plate, leading to the waning of the Great Caribbean Arc and the emplacement of the Lesser Antilles arc.

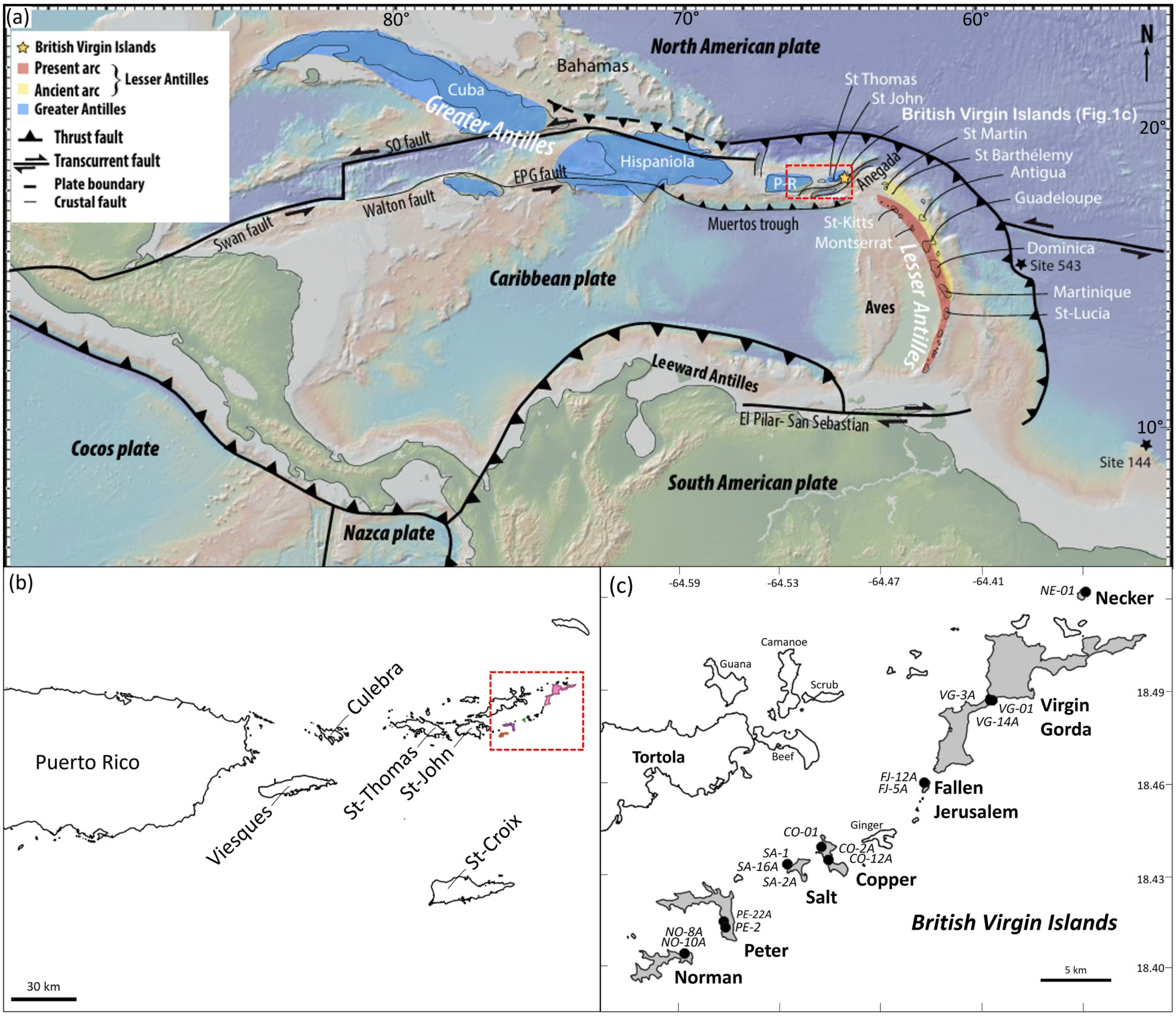

Figure 1. (a) Geodynamic map of the Caribbean plate showing its main boundaries (modified from Cornée et al., 2021). The locations of the Greater and Lesser Antilles archipelagos are indicated as well as the active and extinct volcanic arcs along the Lesser Antilles. Black stars: locations of the "Leg DSDP 78 Site 144" and "Leg DSDP 78 Site 543" (Carpentier et al., 2008); SO fault: Septentrional Oriente fault; EPG fault: Enriquillo Plantain Garden fault. Yellow star: location of the British Virgin Islands. The red dashed square is the inset of (b). (b) Enlargement of the Puerto-Rico/Virgin Islands area. Red dashed square is the inset of (c). (c) Zoom of the study area showing the location of the 15 samples studied.

Arc rocks exposed on the Greater Antilles islands, in the northern Caribbean region, are mainly characterized by tholeiitic and calc-alkaline series (Hastie, 2009; Iturralde-Vinent, 1998; Kerr et al., 1999; Marchesi et al., 2007; Torró et al., 2017) and locally by alkaline series (Torró et al., 2020). Subduction along the northern Caribbean subduction zone continued until mid-Eocene time (Iturralde-Vinent et al., 2008) and came to an arrest due to collision with the Bahamas Bank of the southern North American margin (Bralower & Iturralde-Vinent, 1997; Gordon et al., 1997). On Cuba, the youngest arc magmatic rocks are uppermost Cretaceous in age, except for some Paleocene magmatic rocks in the far southeast, whereas magmatism continued on Hispaniola, Puerto Rico and the Virgin Islands into the Late Eocene (Hu et al., 2022; Jolly et al., 1998; Joyce, 1991). The Cretaceous arc on Cuba is located surprisingly close to the suture, less than 20 km, which suggests that the original forearc, typically 150–200 km width, was removed by Late Cretaceous or Paleocene subduction erosion (van Hinsbergen et al., 2009). Arc magmatism in the Cuban segment may thus have persisted until the cessation of subduction, but it would then be located offshore southern Cuba. Trace elements and isotopic data from volcanic rocks along a

10.1029/2024GC012057

450 km segment of the Greater Antilles arc indicate that the input of sediments in the arc magmas decreased drastically from east to west (Jolly et al., 2008).

Along the eastern Caribbean plate margin, the Lesser Antilles arc, in the eastern Caribbean region, is characterized by successive tholeiitic and calc-alkaline series, particularly in the northern part of the magmatic arc (Atlas et al., 2022; Bouysse & Westercamp, 1990; Cassidy et al., 2012; Davidson et al., 1993; Toothill et al., 2007). The northern part of the Lesser Antilles shows a dichotomy, with the volcanic arc islands splitting into two distinct subparallel segments extending northward of Martinique Island (Figure 1a). The eastern segment corresponds to the outer extinct arc and is the result of Eocene to Lower Miocene volcanic activity (43–23 Ma) (Allen et al., 2019; Bosch et al., 2022; Bouysse & Westercamp, 1990; Legendre et al., 2018; Montheil, Philippon, Cornée, et al., 2023; Noury et al., 2021). The western segment known as the "inner arc" has been active since the early Pliocene (Bouysse & Westercamp, 1990; Favier et al., 2019; Labanieh et al., 2010) (Figure 1). Volcanic rocks of the Lesser Antilles display a wide range of chemical and isotopic compositions typical of oceanic island arcs and define a geochemical gradient along the arc. The central and southern segments of the arc have a greater sedimentary contribution characterized by a "continental" sedimentary component (e.g., Hawkesworth & Powell, 1980; White & Dupré, 1986), which is also evident from the reworking of subducted zircons in the modern arc of Grenada (Rojas-Agramonte et al., 2017). The northern islands show typical oceanic arc compositions and relatively low sediment contributions (Bosch et al., 2022; Cassidy et al., 2012; Davidson et al., 1993; Toothill et al., 2007).

The Virgin Islands are located at the intersection of the southeastern end of the Greater Antilles and the northern portion of the Lesser Antilles. They comprise the American Virgin Islands of St. Thomas, St. John, and St. Croix, as well as the BVI (Figure 1b). In this archipelago, mainly felsic plutonic rocks intruding into the Cretaceous to Paleocene, primarily volcanogenic turbiditic country rocks, are exposed (Speed et al., 1979; Whetten, 1966). The plutons consist of diorite, granodiorite, and occasional gabbro (10%) (Longshore, 1965). Recent paleomagnetic data reveal that the Virgin Islands were part of a large tectonic block that extended from Puerto Rico to Guadeloupe (Montheil, 2023; Montheil, Philippon, Münch, et al., 2023). This block underwent counterclockwise rotation of at least ∼45° between the Late Eocene and Late Miocene, likely as part of a forearc sliver that moved around the northeastern corner of the Caribbean Plate. The sliver was dissected by faults, such as those that formed the Anegada Trough during the Miocene (Figure 1a). The plutons of the Virgin Islands were exhumed during that time (Román et al., 2021), likely due to trench-parallel extension associated with the bending of the forearc sliver around the curved plate boundary (Montheil, 2023).

3. Material and Analytical Methods

This study was carried out using drill microcores and macroscopic samples collected as part of L. Montheil's PhD thesis (Montheil, 2023). A set of 13 cores and three hand samples was selected to represent the diversity of the segment of the seven BVI studied (Figure 1c). From NE to SW the samples are distributed as follows: a volcanic one from Necker, and 15 plutonic rocks: three from VG, two from FJ, three from Copper, three from Salt, two from Peter, and two from Norman. A list of the samples studied, and the type of analysis carried out on each sample is available in Table S1 in Supporting Information S1.

A set of thin (30 μm) and thick (80 μm) sections was produced to perform petrographic analyses, thermobarometrical analyses, and accessory mineral geochronology. In addition, 15 samples were grounded in an agate mortar to obtain whole-rock powders for geochemical analyses (major and trace elements and Pb, Sr, Nd, and Hf isotopes). Moreover, the three hand samples (NE-01, SA-1, CO-01) underwent mineral separation to concentrate heavy minerals (zircon, titanite and apatite) for U-Pb geochronology. U-Pb geochronological and geochemical measurements (major, trace and isotopes) were performed using the AETE-ISO regional facility of the OSU OREME from the University of Montpellier.

3.1. Petrology

Thirteen thin sections were studied under a polarizing optical microscope to characterize the texture of the rocks observed, the mineralogical assemblages and their relative proportions, enabling the lithology of each sample to be defined (Table S1 in Supporting Information S1).

3.2. Geochronology and Thermometry

3.2.1. U-Pb Geochronology and Trace Elements in Accessory Minerals

U-Pb analyses were performed by LA-ICP-MS (Laser Ablation ICP-MS) on seven representative samples, one from each island (Table S2 in Supporting Information S1). Two analytical approaches were applied. The first one, consisting of "in situ" analyses on thick sections, was carried out on 5 samples (NO-8A; PE-22A; SA-1; FJ-5A; N1). Accessory minerals (zircon, titanite and apatite) were first identified using Back-Scattered Electron in conjunction with Energy Dispersive X-ray analysis (EDX) on a FEI Quanta 200 Field Emission Gun Scanning Electron Microscope (SEM) from the University of Montpellier (France). For three samples (SA-1; CO-01; NE-01), heavy minerals were separated. Following separation, zircon, titanite, and apatite grains were selected under binocular microscope examination, mounted in epoxy resin, and polished to reveal internal structures. The operating conditions were as described by Bruguier et al. (2020) and are only summarized below. Ablation experiments were conducted under ultrapure helium using a 193 nm Teledyne G2 excimer laser coupled to a single collector, sector field, ICP-MS (Element XR) modified by the addition of an 80 m^3/hr primary pump in the interface to enhance sensitivity. The instrument was tuned for maximum sensitivity and low oxide production (ThO/Th at $<1\%$). A pre-ablation step was conducted for each analysis consisting of five pulses with a spot diameter slightly larger than the spot size used for the analyses to clean the sample surface and to reduce surface contamination. The laser was operated at a frequency of 5 Hz and a fluence of 5 J/cm^2 for all minerals. The spot size was 20 μm for zircon, 30 μm for titanite and 50 μm for apatite. The recording time was set to 1 min, with the initial 20 s devoted to the blank signal, and the subsequent 40 s used for ablation of the sample. Reference materials were used to calibrate the Pb/Pb and Pb/U ratios of the unknowns. These include 91,500 (Wiedenbeck et al., 1995) and GJ1 (Jackson et al., 2004) for zircon, NIST612, Durango (Chew et al., 2011), and Madagascar (Thomson et al., 2012) for apatite, and MKED1 (Spandler et al., 2016) for titanite. Data evaluation was performed using Glitter software (van Achterbergh et al., 2001). Dates were calculated using IsoplotR (Vermeesch, 2018) and are quoted in the text at 2σ confidence level. Data are presented in either Wetherill Concordia or Tera-Wasserburg Concordia diagrams at 1σ.

Trace elements in zircon and titanite were also analyzed by LA-ICP-MS using the same single collector ICP-MS (Element XR) as described previously. The laser was operated at a repetition rate of 5 Hz, using a 25 μm spot size and an energy density of 5.5 J/cm^2 for zircon; and at a repetition rate of 5 Hz, using a 20 μm spot size and an energy density of 4 J/cm^2 for titanite. The total analysis time was 120 s with the first 80 s used for background measurement prior to sample ablation. Synthetic glass NIST612 was used for external calibration (Pearce et al., 1997). Internal standard normalization was performed using a stoichiometric value of 32.97 wt.% SiO_2. The accuracy of the analyses was monitored using the 91,500 and GJ1 zircon (values taken from GEOREM preferred values), and was consistently better than 15% (see Table S3 in Supporting Information S1). Data reduction was carried out using the Glitter software package (van Achterberg et al., 2001).

3.3. Thermobarometry on Amphibole

Thermobarometry is used to determine the temperature and pressure of mineral crystallization based on their chemical composition. For example, in amphibole, the total aluminum content is correlated with the pressure at the time of mineral crystallization (Hammarstrom & Zen, 1986). Several models exist for the calibration of the Al-in-amphibole thermobarometer. In this study, we used the WinAmptb software (Yavuz & Döner, 2017) to calculate amphibole crystallization pressure using various geobarometers.

Polished thin sections were coated with carbon to determine the major element compositions of amphibole and plagioclase using a JEOL JXA-8230 microprobe equipped with five wavelength-dispersive X-ray spectrometers (WDS) at the *Unidad de Microanálisis* of the *Instituto de Geofísica Unidad Morelia, UNAM*. All analyses were conducted at an acceleration voltage of 15 keV, with a focused beam of 10 nA and a counting time of 20–30 s. Natural minerals were used as standards. Analyses were performed on amphibole and plagioclase rims that appeared to be in textural equilibrium with the surrounding mineral assemblage. We measured the composition of hornblendes for SiO_2, TiO_2, Al_2O_3, FeO*, MgO, MnO, CaO, Na_2O, K_2O, F, and Cl. For the feldspars, we measured SiO_2, Al_2O_3, FeO*, MgO, MnO, CaO, Na_2O, and K_2O. We present pressures computed using WinAmptb (Yavuz & Döner, 2017) using six different geobarometric calibrations that are valid for most of our whole-rock and hornblende compositions. To estimate depth from the computed pressures, a crustal density of

2,700 kg/m^3 and a gravitational acceleration of 9.81 m/s^2 were used. Thermobarometrical data, including standards used during EPMA analyses, are presented in Table S4 in Supporting Information S1.

3.4. Major and Traces Elements in Bulk-Rocks

Major element analyses were performed using an iCAP7400® (ThermoFisher) inductively coupled plasma optical emission spectrometer (ICP-OES) at OSU OREME (Montpellier University, France). Bulk rock powders (ca. 50 mg) mixed with lithium tetraborate ($Li_2B_4O_7$), and a wetting agent were fused at 1,000°C in a Katanax X600® electric fusion fluxer. The fused powders were then poured into Teflon beakers containing ca. 10 mL of 10% HNO_3 and subsequently diluted in 200 ml HNO_3 shortly before analysis. Certified reference materials (BE-N: basalt, UB-N: serpentinite, BHVO: Hawaii basalt, MAG: marine sediment and G2: granite) and blanks were prepared in the same way and used for calibration. Loss on ignition (LOI) was measured using ∼1g of bulk-rock powder heated first to 100°C for 2 hr and then to 1,000°C for 1 hr. Results, expressed in oxide weight percent, are presented in Table S5 in Supporting Information S1.

Trace element analyses were performed using an Agilent 7700x® quadrupole ICP-mass spectrometer at the AETE-ISO platform (OSU OREME, Montpellier University, France). Bulk-rock powders (ca. 50 mg) were dissolved twice in a mixture of HF (48%), HNO_3 (13N) and $HClO_4$ (70%) for 48 hr on a hot plate at 140°C. These dissolutions were followed by three successive evaporation steps at increasing temperature and decreasing $HClO_4$ volume. The aim of these evaporation steps was to eliminate any fluorine and chlorine residues to avoid possible interferences and leaching of HFSE (namely Nb, Ta, Zr, and Hf) from the ICP-MS tubing system and glassware during the analysis. Dry samples were then diluted in 2% HNO_3 to a sample-solution weight ratio of 1:4,000. Internal standardization was conducted using an ultrapure solution enriched in In and Bi, which was used to correct matrix effects and instrument-related mass-dependent sensitivity variations occurring during analytical sessions. Certified reference materials (BE-N, UB-N, and BHVO) were prepared in the same way (except for the dilution factor specific to each standard) and used to verify analytical accuracy. Calibration was performed using multi-element solutions prepared daily from mono-elemental solutions. The raw data obtained were processed using custom Excel macros to correct the data for various interferences. The results of trace element analyses on bulk-rocks are presented in Table S5 in Supporting Information S1.

3.5. Pb-Sr-Nd-Hf Isotopes

3.5.1. Hafnium Isotopes on Zircon

For two samples mounted in epoxy resin (CO-01 and SA-1), laser ablation split-stream analyses (LASS-ICP-MS) were performed to simultaneously obtain U/Pb dates and Hf isotopic ratios of zircon. For Hf/U-Pb split-stream analyses on zircon, the analytical parameters include a 50 μm spot size, a 5 Hz repetition rate and an energy density of 5.5 J/cm^2. After the sample cell, the aerosol (sample + He-N_2) was split by a Y-connector, directing the two streams are directed to a multicollector ICP-MS (Neptune+) and to a single collector ICP-MS (Element XR). U-Pb analyses on the HR-ICP-MS followed the same measurement protocol described above in Section 3.2. For Hf analyses on the MC-ICP-MS, the recording time was 80 s, with the first 40 s devoted to on-peak background measurement followed by 40 s for measuring approximately 40 ratios using a 1.04 s integration time. All isotopes (including Yb, Lu, and Hf isotopes) were measured on Faraday cups equipped with 10^{11} Ω resistors, covering masses ^{171}Yb through ^{179}Hf. Raw data were reduced off-line following the procedure described in reports of Bruguier et al. (2020) including mass bias correction and correction for ^{176}Yb and ^{176}Lu interferences on ^{176}Hf. Standard zircon materials—91,500 (Wiedenbeck et al., 1995), GJ1 (Jackson et al., 2004), and Plesovice (Sláma et al., 2008)—were analyzed each five unknowns with reference ^{176}Hf/^{177}Hf values taken from Blichert-Toft (2008), Morel et al. (2008), and Sláma et al. (2008), respectively (Table S6 in Supporting Information S1).

3.5.2. Strontium, Nd, Pb, and Hf on Bulk-Rock

Whole-rocks were purified in the ISOTOP-MTP laboratory at Geosciences Montpellier, and the results are presented in Table S7 in Supporting Information S1. Bulk-rock powders (ca. 200 mg) were leached in 6N HCl at 110°C for 1 hr and then rinsed three times with ultrapure H_2O to eliminate any trace of alteration. The powders were then put on a hot plate at 140°C for 72 hr with13 N HNO_3. After drying, a mixture of concentrated HF (48%) and 13N HNO_3 was added and placed in Teflon® bomb containers in an oven for 72 hr at 195°C. This type of acid digestion under pressure is essential to ensure the complete dissolution of accessory minerals known to be difficult to dissolve, such as zircon. The purification chemistries for Pb, Sr, Nd, and Hf followed the modified procedure of Richard et al. (1976), Manhes et al. (1978), Pin et al. (1994), and Connelly et al. (2006). Pb-Sr-Nd-Hf isotope analyses were performed using a Neptune Plus® (ThermoFisher) MC-ICP-MS at the AETE-ISO platform facilities (Montpellier University). Certified reference materials (BE-N and G-2) were prepared in the same way and yielded the following results: $^{87}Sr/^{86}Sr = 0.703739 \pm 04$ (2σ) and 0.709300 ± 42 (2σ); $^{143}Nd/^{144}Nd = 0.512885 \pm 05$ (2σ) and 0.512451 ± 67 (2σ); $^{176}Hf/^{177}Hf = 0.282940 \pm 01$ (2σ) and 0.282527 ± 01 (2σ); $^{206}Pb/^{204}Pb = 19.2377 \pm 04$ (2σ) and 18.4059 ± 05 (2σ), $^{207}Pb/^{204}Pb = 15.5932 \pm 04$ (2σ) and 15.6237 ± 06 (2σ), $^{208}Pb/^{204}Pb = 39.0299 \pm 15$ (2σ) and 38.8488 ± 17 (2σ) for BE-N and G-2, respectively.

During the analyses, external standards NBS-981; NBS-987; JMC-321 and Ames Rennes-Nd; JMC-475 and Ames Rennes-Hf were analyzed in bracketing mode for Pb, Sr, Nd, and Hf respectively. The average standard values are detailed below. NBS981 Pb standards were routinely analyzed in bracketing mode ($n = 8$) and yielded the following results: $^{206}Pb/^{204}Pb = 16.9299 \pm 0.06$; $^{207}Pb/204Pb = 15.4820 \pm 0.08$; $^{208}Pb/204Pb = 36.6706 \pm 40$ (true values: 16.9356; 15.4891; 36.7006 respectively), with a reproducibility better than 110 ppm. For the NBS-987 Sr reference material, the measured average value was $^{87}Sr/^{86}Sr = 0.710245 \pm 6$ (2σ) ($n = 10$) (true value: 0.701243–0.710250, $n = 2{,}345$; Jochum et al., 2005); for the AMES Rennes-Nd $^{143}Nd/^{144}Nd = 0.511963 \pm 17$ (2σ) ($n = 5$) (true value: 0.511961 ± 13 (2σ), $n = 50$; Chauvel & Blichert-Toft, 2001); for JMC-321 Nd $^{143}Nd/^{144}Nd = 0.511108 \pm 29$ (2σ) ($n = 8$) (true value: 0.511092 ± 10, $n = 345$, inter-laboratory compilation); for the AMES-Rennes Hf $^{176}Hf/^{177}Hf = 0.282163 \pm 7$ (2σ) ($n = 8$) (true value: 0.282160 ± 1 (2σ), $n = 50$; Chauvel & Blichert-Toft, 2001) and for JMC-475 $^{176}Hf/^{177}Hf = 0.282160 \pm 3$ (2σ) ($n = 6$) (true value $^{176}Hf/^{177}Hf = 0.282170$, $n = 487$; Jochum et al., 2005).

Lead, Sr, Nd, and Hf isotopic ratios were corrected for in situ radioactive decay effects based on the ages obtained in this study.

4. Results

4.1. Petrological Description

Sixteen magmatic samples were selected, among which 15 are plutonic rocks and 1 is a volcanic rock. These samples show no evidence of significant deformation. Thin sections were available for 13 samples. A summary of the mineralogical assemblages for each studied sample is presented in Table S1 in Supporting Information S1.

The different lithologies are described from northeast to southwest across the BVI archipelago, starting with plutonic and then volcanic rocks. For all studied plutonic rocks, the mineral assemblage is relatively homogeneous and mainly consists of feldspars, quartz, amphibole (green hornblende), opaques (magnetite, ilmenite) and accessory minerals (zircon and/or titanite and/or apatite). Additionally, biotite or pyroxene is also present in some samples.

On VG, two samples have been studied. Sample VG-01 is a diorite with amphiboles and feldspars in similar proportion (∼45% each). Sample VG-14A is a coarse-grained gabbro with feldspars (45%) and a high quantity of ferromagnesian minerals, largely dominated by amphiboles (40%) with scarce pyroxenes (Figures 2a and 2b). On FJ Island, two samples were selected. Sample FJ-5A, a quartz-monzodiorite, shows a coarse-grained texture dominated by feldspars (45%), quartz (20%), amphiboles (15%), and biotite (10%) (Figures 2c and 2d). Sample FJ-12A, a monzodiorite, displays a finer grain size than FJ-5A and the following assemblage: feldspars (35%), amphiboles (25%), biotite (25%), and oxides (10%). On Copper Island, two samples were selected. The diorite CO-01 is mainly composed of feldspars (50%), amphiboles (25%), biotite (15%), quartz (5%), and oxides (5%) with a grain size larger than 2 mm (Figures 2e and 2f). The gabbro-diorite CO-2A displays the following assemblage: feldspars (60%), biotite (25%), amphiboles (5%), quartz (5%), and oxides (5%) with grain sizes between 0.5 and 4 mm. On Salt Island, a quartz-diorite (SA-1) and a gabbro (SA-2A) were selected. Sample SA-1 is mainly composed of feldspars (45%), quartz (20%), amphiboles (20%), biotite (10%) and some oxides (Figures 2g and 2h). The gabbro SA-2A, contains up to 50% feldspars, 20% of amphibole, 15% of biotite and some quartz and oxides. Two quartz-monzonites (PE-2) and (PE-22A) were sampled on Peter Island and contain a very similar mineralogical assemblage with feldspars (60%), amphiboles (∼15–20%), quartz (∼10%–20%) and some oxides. Finally, on the southernmost island of Norman, two samples were studied. Sample NO-10A is a fine-grained diorite mainly composed of feldspars (60%), amphiboles (20%), biotite (5%), quartz (5%), and oxides (5%). The quartz-diorite NO-8A is composed of feldspars (50%), amphibole (20%), quartz (20%), and oxides

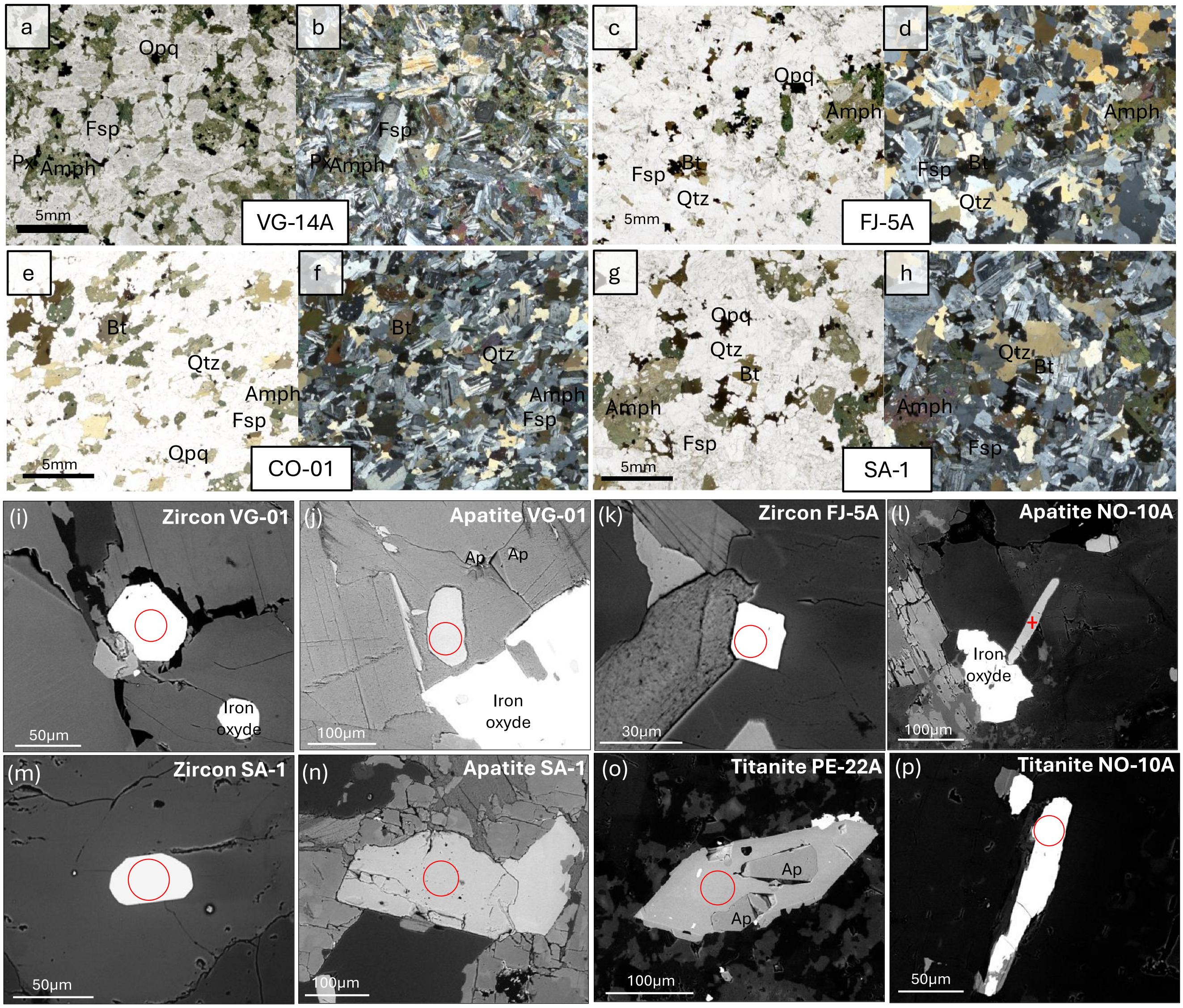

Figure 2. (a–h) Representative thin section microphotographs in natural (a–g) and polarized modes (b–h) of a selection of four samples. (a–b) gabbro VG-14A; (c–d) quartz-monzodiorite FJ-5A; (e–f) diorite CO-01; (g–h) quartz-bearing diorite SA-1. Abbreviations are as follows: Fsp: feldspars; Amph: amphibole; Qtz: quartz; Px: pyroxene; Bt: biotite; Opq: oxides. (i–p) Selected Scanning Electron Microscope microphotographs of accessory minerals (zircon, titanite, and apatite) identified in the different samples. Red circles correspond to the size of the laser spot used for U-Pb analysis. Scale is indicated in each microphotograph. Abbreviations are as follows: Zr: zircon; Ti: titanite; Ap: apatite; Opq: oxides.

(5%). In general, the studied rocks show a very limited degree of alteration, but some traces of sericitization of plagioclase and/or chloritization of biotite can be locally observed in few samples.

Additionally, NE-01 was sampled on Necker Island at the northern tip of the archipelago. It is the only volcanic rock in the present study and exhibits a greenish matrix with destabilized minerals such as quartz and feldspars.

4.2. U-Pb Geochronology and Geochemistry of Accessory Minerals

Accessory minerals (zircon, titanite and apatite) were dated either in situ using thick sections (six samples) or from selected grains mounted in epoxy resin (three samples). In all samples, zircon grains are euhedral with sharp terminations (Figures 2i–2m), and their sizes range from less than 25 μm (FJ-5A, Figure 2k) to approximately 80 μm (Figures 2i–2m). These morphological features suggest crystallization from a melt, indicating a magmatic origin. Apatite and titanite grains are also euhedral, typically larger than zircon grains, reaching up to ∼300 μm in size (Figures 2j–2p). U-Pb results are presented following the alignment of the islands, that is, from NE to SW. In

10.1029/2024GC012057

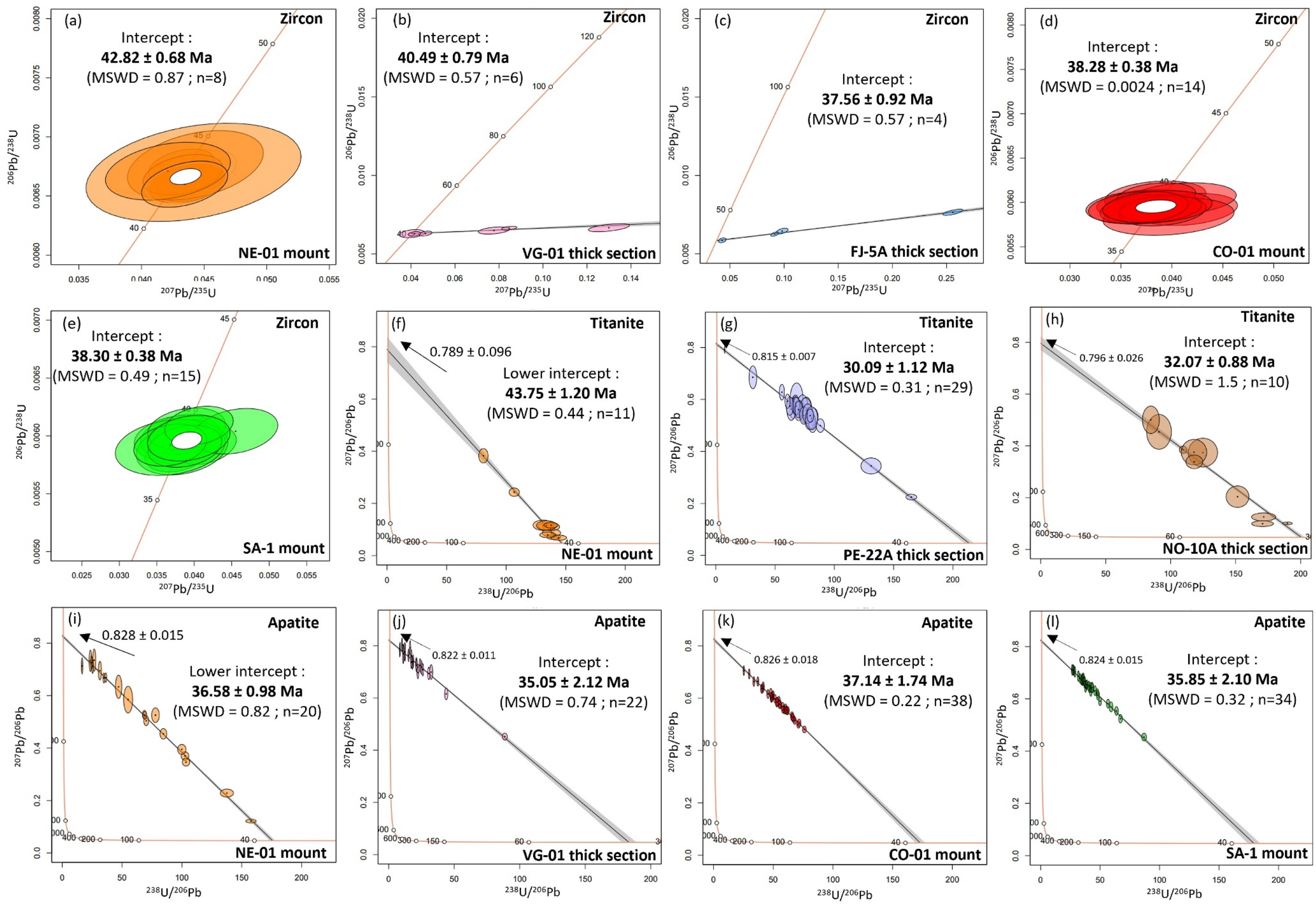

Figure 3. Concordia (zircon) and Tera-Wasserburg (titanite and apatite) U-Pb diagrams obtained for the different accessory minerals analyzed: zircon (a–e), titanite (f–h) and apatite (i–l). MSWD = Mean Square of Weighted Deviation; n = number of analyses; ellipses are given at $\pm 1\sigma$ error and absolute dates are given at 2σ confidence level. The common lead intercept is indicated by a narrow in the Terra Wasserburg diagrams. The type of analysis (epoxy mount or thick section) is specified.

total, 12 U-Pb ages were obtained from zircon, titanite, or apatite (Figures 3a–3l). The sample from Necker Island (NE-01) yields the oldest U-Pb titanite date of the present study, with a titanite age of 43.75 ± 1.20 Ma (Mean Square of Weighted Deviation (MSWD) = 0.4; Figure 3f). This age is indistinguishable from the more accurate U-Pb zircon age of 42.82 ± 0.68 Ma (MSWD = 0.9; Figure 3a) but significantly older than the apatite date of 36.58 ± 0.98 Ma (MSWD = 0.8; Figure 3i) obtained for this sample. One zircon grain (see Table S2 in Supporting Information S1) yielded a slightly older age at 46.3 ± 2.8 Ma (2σ), suggesting the presence of an inherited component in the basement of Necker Island. Sample VG-01 from VG Island, located slightly farther south, yields similar U-Pb zircon and apatite ages, within analytical uncertainty, to those obtained on sample NE-01 with ages of 40.49 ± 0.79 Ma (MSWD = 0.6; Figure 3b) and 35.05 ± 2.12 Ma (MSWD = 0.7; Figure 3j) for zircon and apatite, respectively. Samples from FJ-5A, Copper (CO-01) and Salt (SA-1) islands, located in the central part of the archipelago, yield comparable U-Pb zircon ages of 37.56 ± 0.92 Ma (MSWD = 0.6; thick section; Figure 3c), 38.28 ± 0.38 Ma (MSWD = 0.1; mount; Figure 3d) and 38.30 ± 0.38 Ma (MSWD = 0.5; mount; Figure 3e), respectively. U-Pb apatite ages have also been obtained for the Copper and Salt islands, yielding ages of 37.14 ± 1.74 Ma (MSWD = 0.2) and 35.85 ± 2.10 Ma (MSWD = 0.3), respectively (Figures 3k and 3l). In both cases, these dates are similar to those obtained for co-existing zircon, considering the analytical uncertainties. One zircon grain, however, is slightly but significantly older, with an age of 41.1 ± 1.2 Ma (2σ), suggesting the presence of an older component in the basement of Salt Island. Finally, samples from Peter (PE-2) and Norman (NO-8A) islands, located at the southwestern end of the archipelago, were dated using titanite only, yielding ages of 30.09 ± 1.12 Ma (MSWD = 0.3) and 32.07 ± 0.88 Ma (MSWD = 1.5), respectively (Figures 3g and 3h). These ages are considered similar given their respective uncertainties.

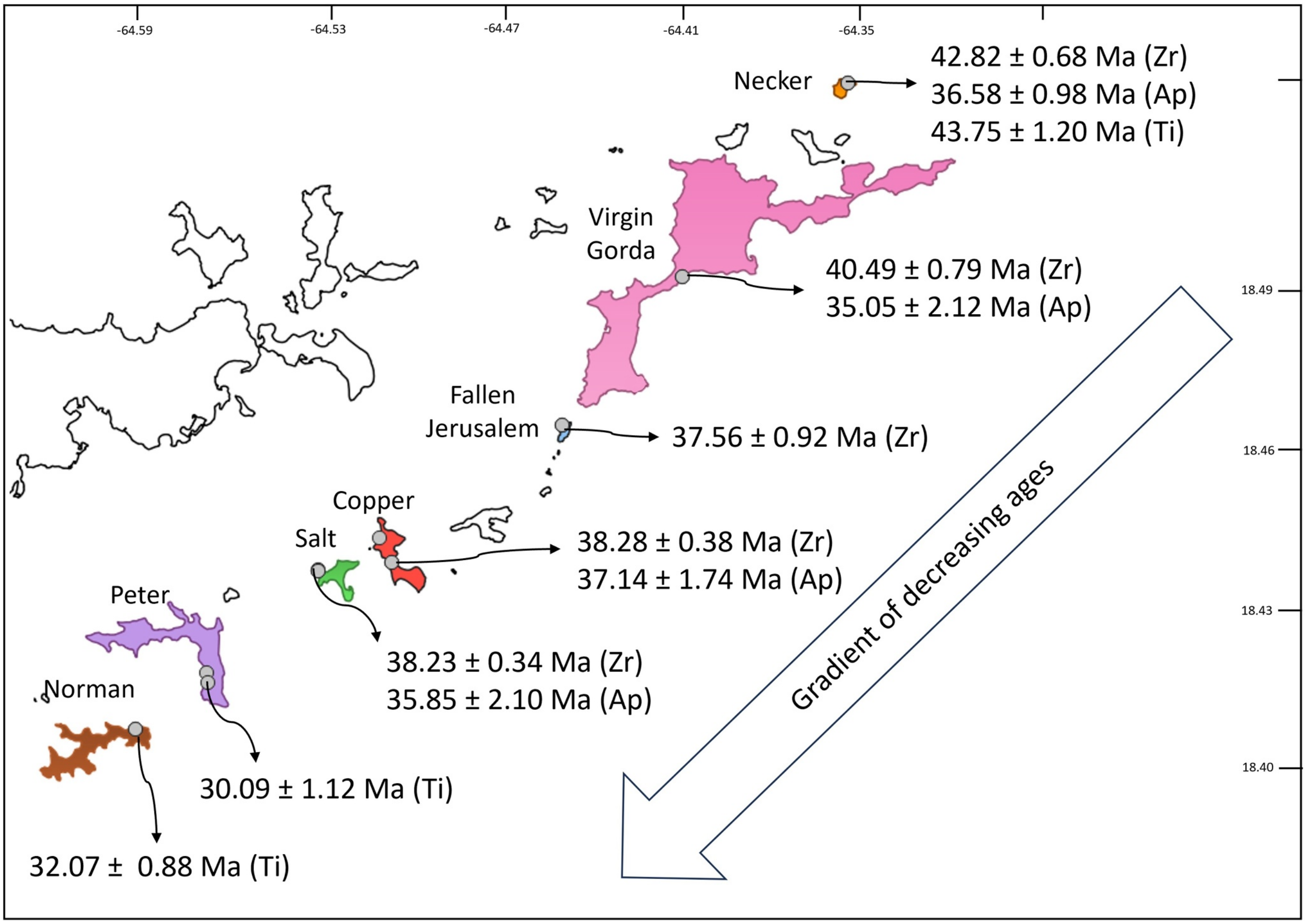

Figure 4. The U-Pb ages obtained on zircon (Zr), titanite (Ti), and apatite (Ap) (this study) are reported as a function of the sample's location.

Regionally, the Virgin Island archipelago exhibits a NE to SW decreasing ages trend (Figure 4). This age gradient, spanning from ca. 43.75 Ma to ca. 30.09 Ma, is interpreted to reflect a magmatic/volcanic activity that lasted approximately 13 Myr. The activity began in the northeastern part of the archipelago at Necker Island and gradually migrated southwestward to Peter Island (see Table S2 in Supporting Information S1).

Zircons from NE-01, VG-01, CO-01, and SA-1 were analyzed for their trace element contents (Table S3 in Supporting Information S1). Overall, the Rare Earth Elements (REE) patterns for the four samples are typical of magmatic zircon, with low La contents, prominent positive Ce anomaly and steep HREE slopes (Yb_N/Gd_N = 16–37; 27–56; 38–72; and 23–43 for NE-01, VG-01, CO-01, and SA-1 respectively). Additionally, the REE patterns are characterized by negative Eu anomalies, suggesting zircon crystallization in an Eu-depleted environment, that is, coeval with or after plagioclase crystallization. The Ti content of zircon in the four samples is relatively consistent, averaging 10.9, 7.0, 7.8, and 8.6 ppm for NE-01, VG-01, CO-01, and SA-1, respectively. Using the Ti-in-Zircon thermometry of Ferry and Watson (2007), the calculated crystallization temperatures of the grains yield values of 753 ± 42°C ($n = 5$), 713 ± 32°C ($n = 5$), 722 ± 24°C ($n = 7$), and 731 ± 34°C ($n = 7$) for NE-01, VG-01, CO-01, and SA-1, respectively (Table S3 in Supporting Information S1). Considering the uncertainties, these temperatures are close similar to one another and are interpreted as the zircon crystallization temperature in the magma.

Titanites grains from PE-2 and NO-8A were analyzed for their trace element contents (Table S3 in Supporting Information S1) to calculate the crystallization temperature using the thermobarometer of Hayden et al. (2008). The calculated temperatures are 817 ± 26°C for PE-2 ($n = 8$) and 680 ± 11°C for NO-8A ($n = 3$).

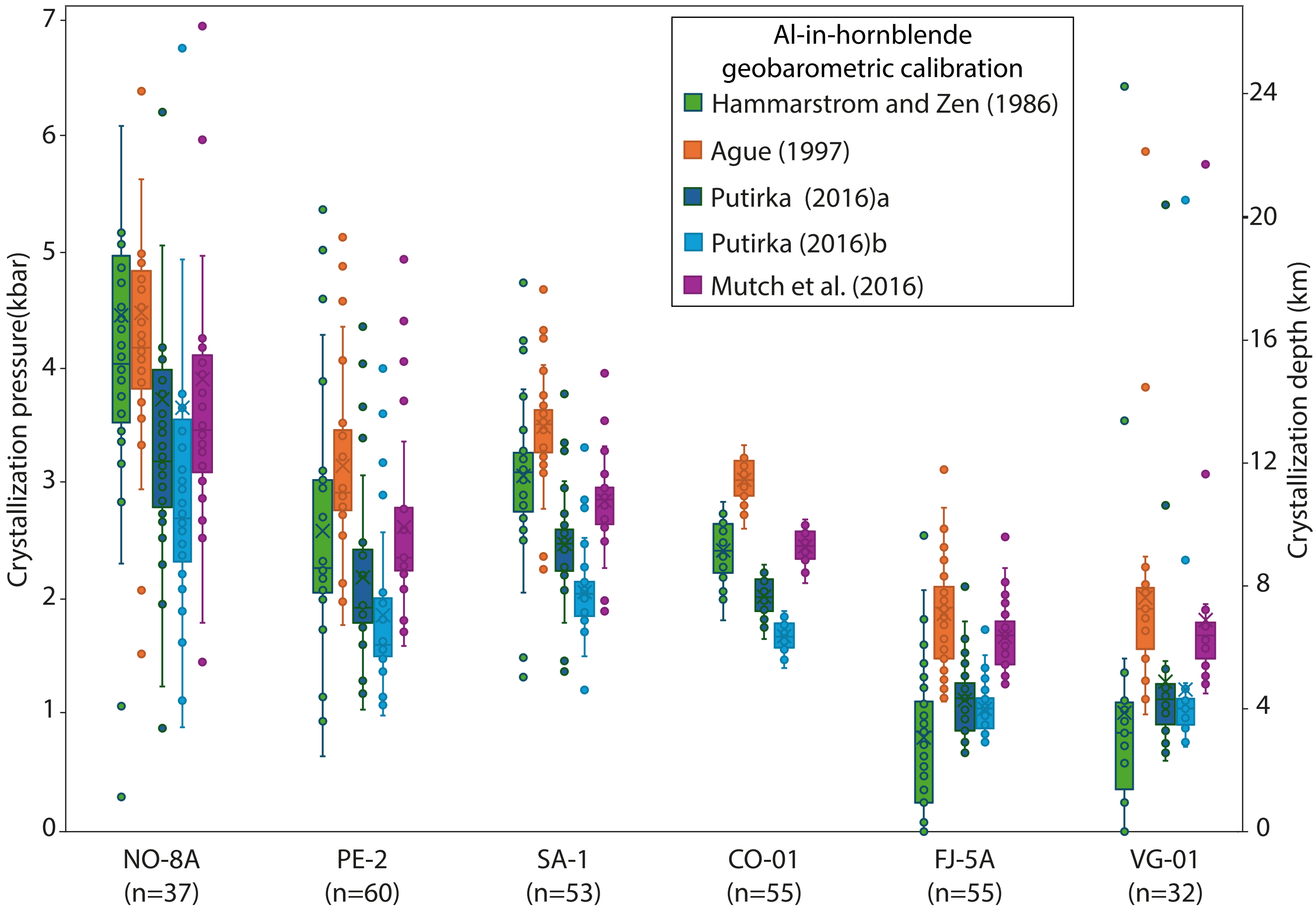

Figure 5. Box and whisker plots of the thermobarometrical data obtained from plutonic rocks on the British Virgin Islands plutonic. Several models have been used for calibration of Al-in-amphibole thermobarometers. The WinAmptb software was used to calculate the crystallization pressure of amphibole using the following geobarometers: dark blue square (Hammarstrom & Zen, 1986); red square (Ague, 1997); green square (Putirka, 2016; equation a); violet square (Putirka, 2016; equation b) and blue square (Mutch et al., 2016). Samples are presented from SW to NE (Norman to Virgin Gorda). The whiskers represent the first and the last quartiles of the data set. The box encompasses the second and third quartiles, with the average and the median values indicated by a line and a cross, respectively. Dots outside the whiskers are considered outliers. Crystallization depth was calculated from the crystallization pressure assuming a crustal density of 2,700 kg/m^3 for the overlying rocks.

4.3. Pressure Constraints

Thermobarometric analyses were performed on the rims of plagioclase and amphibole pairs in apparent textural equilibrium with the rest of the mineral assemblage (Mutch et al., 2016), which contained at least plagioclase, hornblende, alkali-feldspar, quartz, biotite, apatite and Fe- and Ti-oxides. Some plagioclase laths within amphibole (Table S4 in Supporting Information S1) were also analyzed and showed higher crystallization temperatures and pressures in their cores than in their rims, suggesting that the magma was ascending while partially crystallizing. The results from the analyses of mineral rims clearly indicate that the crystallization pressure of the outcropping rocks increases from NE (VG Island) to SW (Norman Island).

For sample VG-01, located at the NE of the archipelago, the Hammarstrom and Zen (1986) calibration is the one yielding the lower and higher crystallization pressures (ranging from 0 to 6.4 kbars), with 50% of the data falling between 0.4 and 1.4 kbars. The median and mean pressures are 0.8 and 1.3 kbars, respectively (Figure 5; Table S4 in Supporting Information S1). Considering all the calculated crystallization pressures for sample VG-01, the mean pressure is 1.5 kbar with a standard deviation of 1.0 kbar (Table S4 in Supporting Information S1).

For sample FJ-5A, crystallization pressures range from 0 (the lowest value obtained using the Hammarstrom and Zen calibration, Table S4 in Supporting Information S1) to 3.1 kbar (the highest value obtained using the Ague (1997) calibration, Table S4 in Supporting Information S1). The median and mean values are similar for

10.1029/2024GC012057

both of the Hammarstrom and Zen (1986) and Ague (1997) geobarometers, with 0.9 and 1.9 kbar, respectively. Considering all the calculated crystallization pressures for sample FJ-5A, the mean pressure is 1.3 kbar with a standard deviation of 0.6 kbar (Table S4 in Supporting Information S1).

For sample CO-01, hornblendes show more reproducible compositional results. The lowest crystallization pressures were obtained using the barometer of Putirka (2016; Equation b), with values ranging from 1.4 to 1.9 kbar and median and mean values of 1.7 kbar. The highest crystallization pressures obtained for sample CO-01 were obtained using the calibration of Ague (1997), with values ranging from 2.6 to 3.3 kbar, and similar mean and median values of 3.0 kbar. Considering all the calculated crystallization pressures for sample CO-01, we obtained a mean pressure of 2.3 kbar with a standard deviation of 0.5 kbar (Table S4 in Supporting Information S1).

Sample SA-1 yielded crystallization pressures generally higher than those obtained for CO-01. Using the geobarometer of Putirka (2016; Equation b), which provides the lowest values, pressions range from 1.2 to 3.3 kbar, with similar median and mean values of 2.1 kbar. For this sample, it is the calibration of Ague (1997), which yields the highest crystallization pressures, ranging from 2.3 to 4.7 kbars and with a median and mean of 3.5 kbars. Considering all the calculated crystallization pressures for sample SA-1, we obtained a mean pressure of 2.8 kbar with a standard deviation of 0.7 kbar (Table S4 in Supporting Information S1).

The sample from Peter Island (PE-2) yielded dispersed results but values comparable to those obtained for CO-01 and SA-1. The lowest crystallization pressures were obtained using the geobarometer proposed by Putirka (2016; equation b), with values ranging between 1.0 and 4.0 kbar, with median and mean values of 1.6 and 1.9 kbar, respectively. The highest values for this sample are provided by the geobarometer of Ague (1997), with values ranging from 1.8 to 5.1 kbar, with median and mean values of 2.9 and 3.2 kbar, respectively. Considering all the calculated crystallization pressures for sample PE-2, we obtained a mean pressure of 2.5 kbar with a standard deviation of 0.9 kbar (Table S4 in Supporting Information S1).

Finally, sample NO-8A from Norman Island, the southwesternmost island of the archipelago, yielded the highest crystallization pressures. As with previous samples, the amphibole barometer calibration of Putirka (2016; Equation b) provides the lowest values, which range between 0.9 and 11.0 kbar, with median and mean values of 2.7 and 3.7 kbar, respectively. The highest values are given by the Hammarstrom and Zen (1986) calibration with pressures ranging from 0.3 to 8.8 kbars and median and mean values of 4.0 and 4.4 kbar, respectively. Considering all the calculated crystallization pressures for sample NO-8A, we obtained a mean pressure of 4.0 kbar with a standard deviation of 1.9 kbar (Table S4 in Supporting Information S1).

Thus, considering a crustal density of 2,700 kg/m^3, the corresponding crystallization depths vary from 15.2 ± 7.2 km at the southwestern end of the archipelago (sample NO-8A) to 5.6 ± 3.9 km at its northeastern end (sample VG-01). These values correspond to the mean and the standard deviation of all crystallization pressures computed using the different calibrations (Figure 5, Table S4 in Supporting Information S1).

4.4. Geochemistry

4.4.1. Major Elements

For the 15 samples studied, the LOI is low to moderate with values ranging from 0.5% to 5.5% (Table S5 in Supporting Information S1), thus reflecting a variable degree of alteration. Low LOI values—that is, less than 2%—indicate very low alteration imprint, which is the case for 13 out of 15 samples. Two samples yield significantly higher LOI values of 3.6% and 5.5% corresponding to the volcanic NE-01 and the gabbro SA-2A, respectively (Table S5 in Supporting Information S1).

The samples define a wide range of SiO_2 variations from 46.5 to 68.2 wt.% (Table S5 in Supporting Information S1). In the Harker diagrams (Figures 6a–6f), using SiO_2 as a differentiation index, the data define linear trends without marked discontinuities. Samples range from mafic, less differentiated rocks like the VG-3A and VG-14A gabbros to highly differentiated felsic rocks such as the PE-22A quartz-monzonite. The total number of alkalis ($Na_2O + K_2O$) ranges from 2.33 to 8.28 wt.% (Table S5 in Supporting Information S1). Overall samples define a positive trend with an increase in alkalis from the least to the most differentiated samples (Figure 6a). A few samples deviate slightly from this general trend (i.e., NE-01, FJ-5A, FJ-12A, SA-16A). The same trend can be observed in the Na_2O versus SiO_2 diagrams (Figure 6c) with a range of values from 2.20 to 4.80 wt.%. In

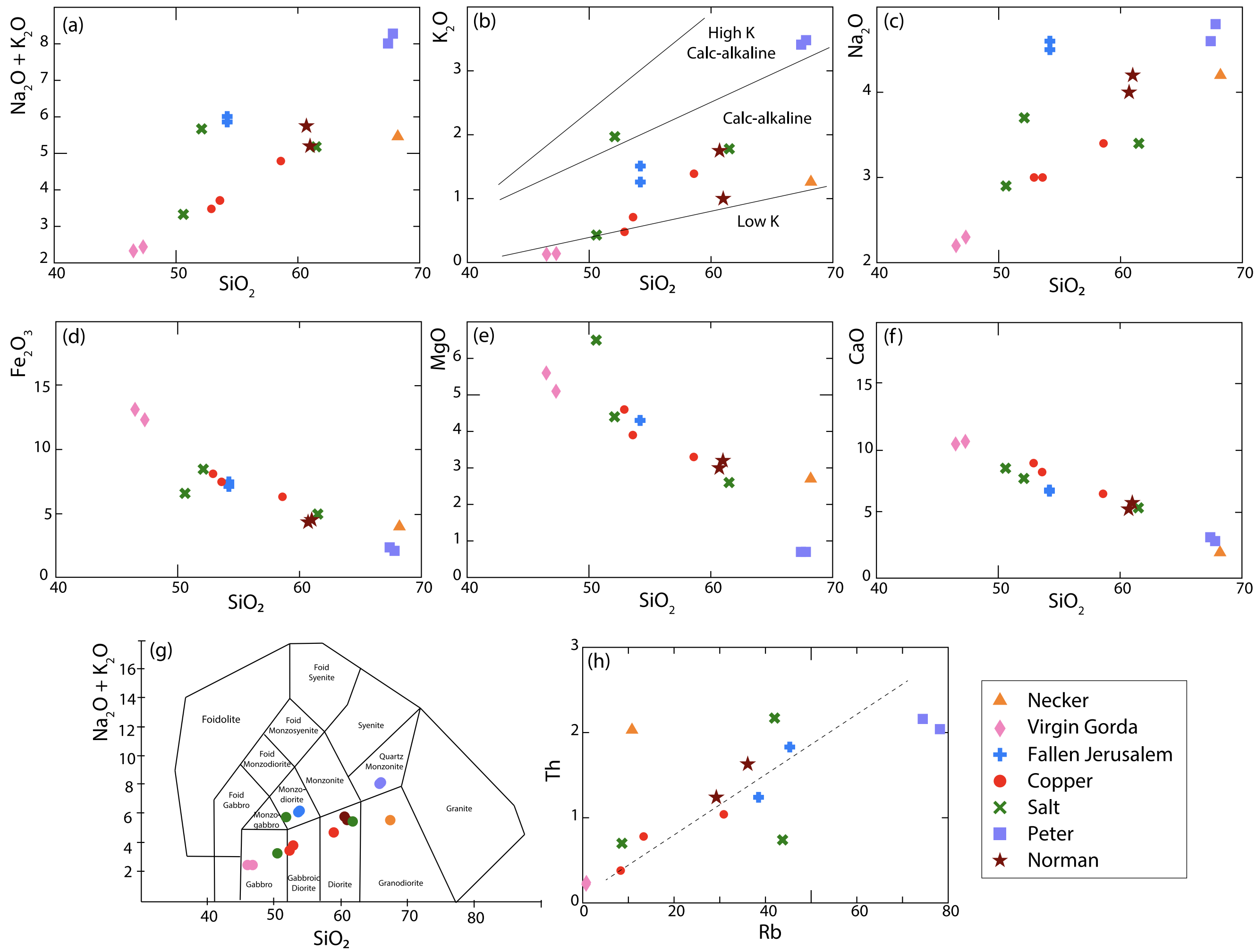

Figure 6. Major element composition (wt.%) for the British Virgin Islands samples. (a–f): Harker diagrams. (a) $Na_2O + K_2O$ (wt.%) versus SiO_2 (wt.%); (b) K_2O (wt.%) versus SiO_2 (wt.%); Are indicated the fields of high K, calc alkaline and low K rocks (Gill, 1981) (c) Na_2O (wt.%) versus SIO_2 (wt.%); (d) Fe_2O_3 (wt.%) versus SiO_2 (wt.%); (e) MgO% (wt.%) versus SiO_2 (wt.%); (f) CaO (wt.%) versus SiO_2 (wt.%). (g) Total alkali versus silica diagram after Middlemost (1994); (h) Th (ppm) versus Rb (ppm). Symbols correspond to the different island's samples.

Figure 6b, except for three samples (one from Salt Island and two from Peter Island), which plot at the lower boundary of the high-K calk-alkaline series, all other samples fall within the field of the calk-alkaline magmatic series. Conversely, Fe_2O_3 (2.30–14.60 wt.%), MgO (0.70–6.50 wt.%) and CaO (2.00–10.70 wt.%) contents decrease as a function of increasing SiO_2, defining a negative correlation trend (Figures 6d–6f). In Figure 6g, the samples range from gabbro to quartz-monzonite following the Middlemost (1994) nomenclature.

4.4.2. Trace Elements

The degree of alteration in the samples was assessed using Figure 6h, where an immobile element (Th) is plotted against a mobile element (Rb). Excluding the NE-01 volcanic sample and the diorites from Norman Island (NO-10A, NO-8A), the remaining samples show a rough Th/Rb correlation, interpreted as reflecting a little imprint of alteration. Therefore, the geochemical characteristics can be considered representative of the magmas' primitive features. The chondrite-normalized REE and primitive mantle-normalized trace element patterns are shown in Figures 7a and 7b. All samples exhibit REE contents enriched by a factor of 10–40 times compared to chondrites, a range commonly observed in Mid-Oceanic Ridge Basalts (MORBs). The samples also show slight to strong enrichment in light REE (LREE) relative to heavy REE (HREE), with La/Yb ratios ranging from 1.16 to 18.08 (Figure 7a, Table S5 in Supporting Information S1). This range narrows significantly, that is, from 1.16 to 6.60, when the differentiated samples from Peter Island are excluded. Subtle differences in the patterns can be observed

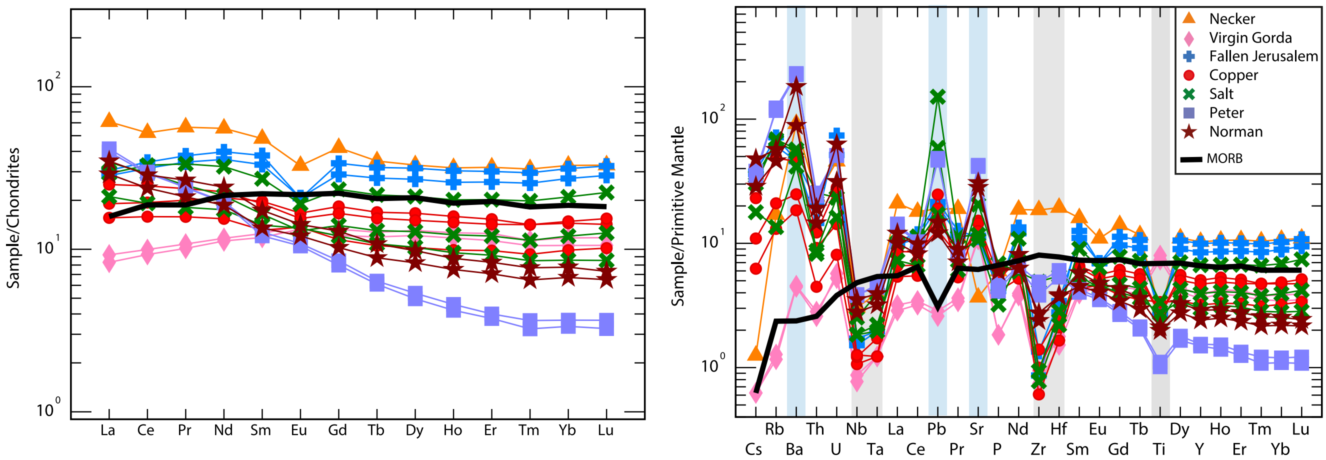

Figure 7. Whole-rock geochemical analyses for the British Virgin Islands samples. (a) Rare Earth Elements normalized to chondrites (McDonough & Sun, 1995). (b) Trace element extended diagram normalized to primitive mantle (Sun & McDonough, 1989). Mobile elements (Ba, Pb, Sr) are highlighted by a blue bar and HFSE (Zr, Hf) + Ti are highlighted by a gray bar. The bold black line corresponds to the average Mid-Oceanic Ridge Basalt (Arevalo & McDonough, 2010).

between the less and more differentiated samples, such as the Eu anomaly, which can be negative, positive, or absent (Figures 7a and 7b). Gabbros from VG differ from the other samples by exhibiting lower LREE/MREE enrichment with the lowest La/Sm ratio (1.13–1.18). The two samples from FJ show nearly flat REE patterns, with La/Yb ratios of 1.44 and 1.53, La/Sm ratios of 1.30 and 1.37, as well as a strong negative Eu* anomaly of 0.58 and 0.67for FJ-5A and FJ-12A, respectively (Figures 7a and 7b). Samples from Copper and Salt islands show close to similar spectra with slight LREE enrichment relative to HREE as expressed by La/Yb ratios ranging from 1.94 to 4.18 and La/Sm ratios from 1.54 to 3.34 (Figures 7a and 7b). Samples from Norman and Peter islands display pronounced LREE/HREE enrichment (La/Yb ranging from 6.38 to 18.08) without discernible Eu anomalies (i.e., 0.95–1.07) (Table S5 in Supporting Information S1) (Figures 7a and 7b). The spectrum of the Necker volcanic sample shows the highest LREE concentration, a marked negative Eu* anomaly (i.e., 0.73) and LREE/HREE enrichment with a La/Yb ratio of 2.73 (Figures 7a and 7b).

Except for the gabbros from VG, the extended primitive mantle-normalized trace element patterns show significant enrichment in incompatible elements, generally attributed to the contribution of fluids (Tatsumi et al., 1986). These enriched patterns are accompanied by strong negative HFSE anomalies in Nb-Ta, Zr-Hf, and Ti, which are commonly used as proxies for subduction environments. Nevertheless, a significantly less marked Zr-Hf depletion is observed in the Peter Island samples compared to the other igneous samples. Furthermore, except for the gabbros from VG and the volcanic sample from Necker Island, all samples show pronounced positive anomalies in Sr and Pb (Figure 7b). Fluid-mobile element/REE ratios, such as Ba/La, range from 14.5 (VG-3A) to 173.2 (PE-2) while Ce/Pb ratios range from 0.72 (SA-16A) to 11.76 (VG-14A).

4.4.3. Isotopes

The results of Pb, Sr, Nd, and Hf isotopes are presented in Table S7 in Supporting Information S1 and Figures 8 and 9. Isotope ratios have been corrected for the effects of radioactive decay over time using the absolute U-Pb ages obtained in this study for each island.

All samples define a very restricted range of variation of initial Pb isotopic ratios, with values spanning from 18.71 to 18.96 for $^{206}Pb/^{204}Pb$, from 15.61 to 15.64 for $^{207}Pb/^{204}Pb$, and from 38.44 to 38.66 for $^{208}Pb/^{204}Pb$. In Figures 8a and 8b, the samples from the BVI plot at the boundary between the domains of global MORB and worldwide pelagic sediments, overlapping with the field defined for Island Arc Basalt (IAB). In Figure 8b, they define a linear trend parallel to the Northern Hemisphere Reference Line (NHRL; Hart, 1984).

However, subtle distinctions exist among the studied samples as seen in the inset of Figure 8b where the samples define a positive trend. The samples from Peter and Norman—the youngest and most differentiated ones—show the highest $^{206}Pb/^{204}Pb$ and $^{207}Pb/^{204}Pb$ ratios while the samples from FJ and Copper Islands show the lowest ratios. In contrast, no clear alignment is apparent in Figure 8a.

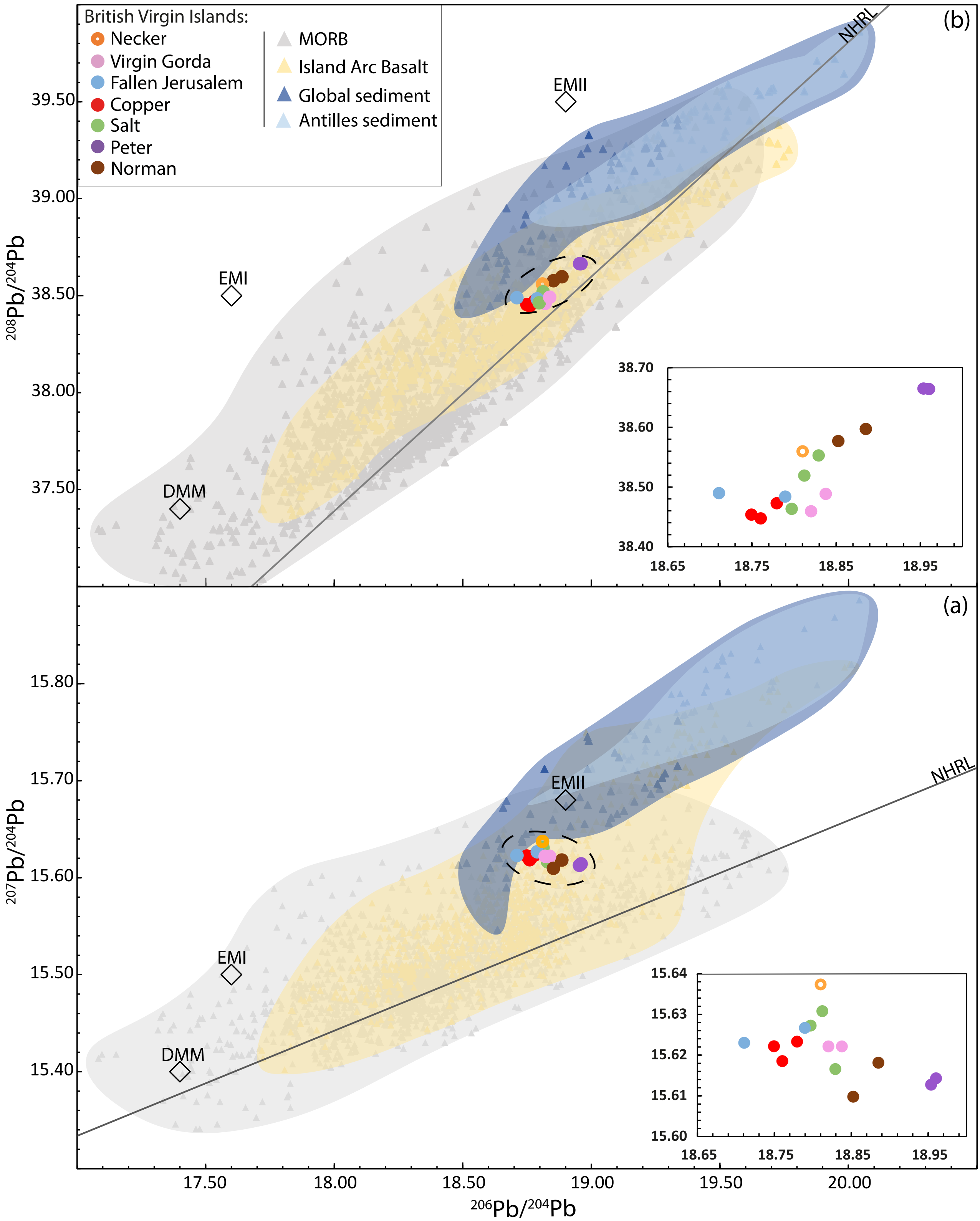
British Virgin Islands:
Necker
Virgin Gorda
Fallen Jerusalem
Copper
Salt
Peter
Norman
MORB
Island Arc Basalt
Global sediment
Antilles sediment
(b)
(a)
NHRL
EMII
EMI
DMM
$^{208}Pb/^{204}Pb$
$^{207}Pb/^{204}Pb$
$^{206}Pb/^{204}Pb$
39.50
39.00
38.50
38.00
37.50
15.80
15.70
15.60
15.50
15.40
17.50
18.00
18.50
19.00
19.50
20.00
38.70
38.60
38.50
38.40
15.64
15.63
15.62
15.61
15.60
18.65
18.75
18.85
18.95

Figure 8.

Furthermore, the calculated values of Δ7/4Pb and Δ8/4Pb, which represent the differences between the $^{207}Pb/^{204}Pb$ and $^{208}Pb/^{204}Pb$ ratios of the samples and the NHRL (Hart, 1984), are positive for all samples. These Δ values reflect the deviation between the measured ratios in the samples and the NHRL, which is considered the correlation line for rocks formed from mantle components. These values range from +6.71 to +10.73 for Δ7/4Pb and from +7.88 to +24.15 for Δ8/4Pb (Table S7 in Supporting Information S1).

Fourteen of the 15 studied samples show a limited range of $^{87}Sr/^{86}Sr_i$ ratios narrowly ranging between 0.70268 and 0.70408, with corresponding εSr_i values ranging from −25.1 to −5.4 (Table S7 in Supporting Information S1). The only sample deviating from this trend is the volcanic rock from Necker Island, which yields an $^{87}Sr/^{86}Sr_i$ ratio of 0.70512 and a corresponding εSr_i value of +9.5. This positive εSr value may result from a slight effect of hydrothermal alteration and/or surface weathering, consistent with its elevated LOI value (3.6 wt.%, Table S7 in Supporting Information S1) and with its volcanic origin. Nevertheless, all studied samples yield Sr isotopic ratios in good agreement with a subduction environment (Figure 9a). Neodymium isotopic ratios are less sensitive to alteration processes and are thus more reliable for characterizing the magmas source reservoirs. The $^{143}Nd/^{144}Nd_i$ values display a broader range comprised between 0.51280 and 0.51307, with corresponding εNd_i values spanning from +3.8 to +9.5 (Table S7 in Supporting Information S1). Samples CO-2A from Copper Island and NE-01 from Necker Island yield the most radiogenic Nd isotopic compositions—that is, the closest to the DMM component—with values at +8.9 and + 9.5, respectively. In the Nd-Sr correlation diagram (Figure 9a), all samples, except NE-01, fall within the depleted area relative to Bulk Earth (CHUR) and define a roughly inverse correlation. The domain defined by the BVI samples overlaps with the island arc basalt (IAB) field located between the MORB mantle and the global pelagic sediment fields.

The $^{176}Hf/^{177}Hf_i$ ratios show a narrow range comprised between 0.28308 and 0.28315, with corresponding εHf_i values ranging from +11.4 to +14.1 (Table S7 in Supporting Information S1). In Figure 9b, a slight negative correlation is observed among the BVI samples, with all the samples extending from the MORB field to the global pelagic sediment field and overlapping the island arc basalts (IAB) domain.

4.4.4. In Situ Hf Isotope Analyses on Zircon

Hf isotopes were measured on zircons mounted in epoxy resin for the SA-1 and CO-01 samples. The εHf_i values are positive ranging from +13.6 to +14.7 for SA-1 and from +12.7 to +15.1 for CO-01 (Table S6 in Supporting Information S1, Figure 10). It is noteworthy that the range defined for sample CO-01 is broader than that for sample SA-1 although the two ranges do overlap. The εHf values of the corresponding whole-rock samples (+12.7 for CO-01 and +13.4 for SA-1) are slightly below or within the, considering the uncertainties, range of zircon-bearing values. These values plot above the CHUR line and just below the depleted mantle line, indicating a significant involvement of juvenile mantle material in the magmatic source (Figure 10).

5. Discussion

5.1. Timing of the Formation of the British Virgin Islands Archipelago and Its Temporal Relationship With the Greater and Lesser Antilles Arcs

The oldest age obtained in this study is from Necker Island, located in the northeastern part of the archipelago, with a titanite U-Pb age of 43.7 ± 1.2 Ma, which is indistinguishable within errors, from the zircon U-Pb crystallization age of 42.97 ± 0.26 Ma from the same sample. Further south, on VG Island, a diorite was previously dated at 43.6 ± 0.1 Ma using zircon fractions (Schrecengost, 2010). We thus considered that the onset of magmatic activity in the BVI archipelago occurred during the Lutetian. On VG Island, the diorite VG-01 yields a zircon U-Pb crystallization age of 40.5 ± 0.8 Ma. A slightly younger crystallization age of 37.60 ± 0.05 Ma was also obtained by Schrecengost (2010) for a granodiorite located at the southwestern extremity of the VG Island. This latter age is in very good agreement with the 37.56 ± 0.9 Ma zircon U-Pb age obtained for the quartz-

Figure 8. Initial Pb isotope correlation diagrams. (a) $^{207}Pb/^{204}Pb$ ratio versus $^{206}Pb/^{204}Pb$ ratio, and (b) $^{208}Pb/^{204}Pb$ ratio versus $^{206}Pb/^{204}Pb$ ratio. Reported for comparison: Mid-Oceanic Ridge Basalt (MORB) (gray) and arc oceanic basalt (yellow) from the Georoc database http://georoc.mpch-mainz.gwdg.de/georoc/; global pelagic sediments (dark blue) from Plank and Langmuir (1998); Antilles sediment composition (light blue) estimated from sediments of boreholes "Leg DSDP 78 site 144" and "Leg DSDP 78 site 543" from Carpentier et al. (2008); Depleted MORB Mantle (Workman & Hart, 2005), EM1 and EM2 (Enriched Mantle Type-1 and Type-2; Hart, 1984). NHRL: Northern Hemisphere Reference Line (Hart, 1984). Insets show a zoom of the values obtained for the British Virgin Islands samples in this study.

10.1029/2024GC012057

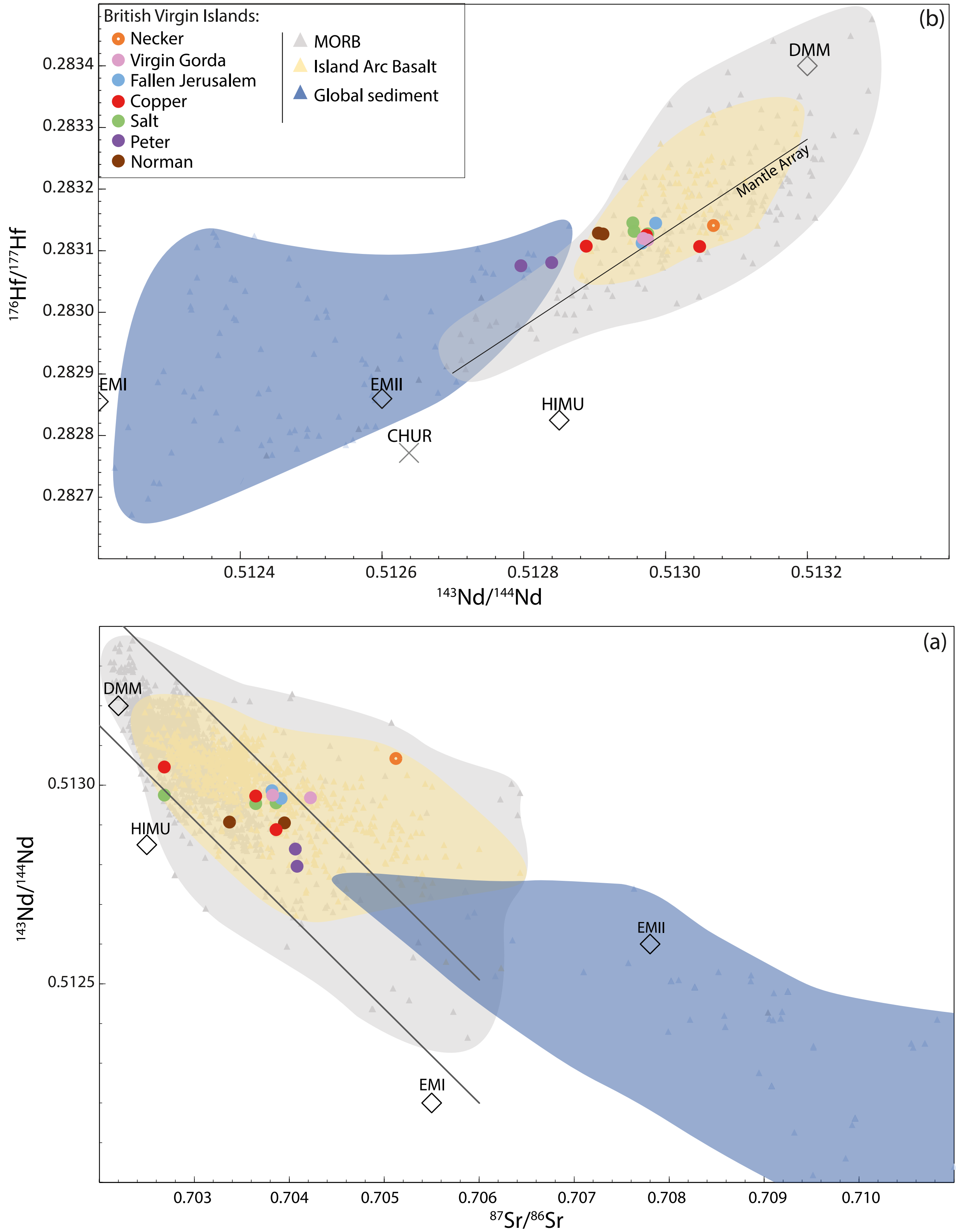

Figure 9.

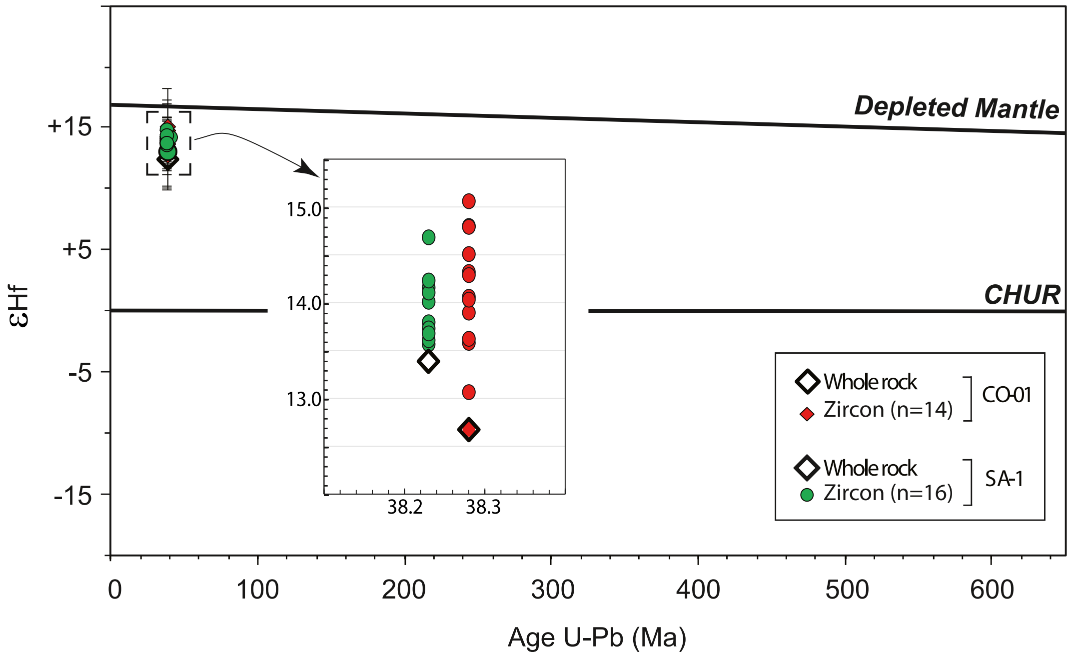

Figure 10. Plot of εHf versus U-Pb age (Ma) for zircon grains from the CO-01 and SA-1 samples. The εHf values of the corresponding whole-rock along with the evolution lines (solid black) for the Depleted Mantle and CHUR (Bouvier et al., 2008; Chauvel & Blichert-Toft, 2001) are shown for comparison.

monzodiorite FJ-5A from FJ Island, located less than one km southwest of the southern tip of VG Island. Additionally, samples CO-01 and SA-1 from the Copper and Salt Islands provide similar zircon U-Pb ages of 38.27 ± 0.38 and 38.23 ± 0.34 Ma, respectively. The youngest U-Pb ages obtained in this study are from the southwesternmost islands, that is, Norman and Peter, which yielded titanite ages of 32.1 ± 0.9 Ma for a diorite and 30.1 ± 1.1 Ma for a quartz-monzonite, respectively. These significantly younger ages are corroborated by the Oligocene zircon U-Pb age of 30.7 ± 0.1 Ma previously determined for a diorite sampled on Peter Island (Schrecengost, 2010). Together with previous studies, U-Pb results from the seven samples collected across the BVI, from the northeastern to the southwestern ends of the archipelago, support a magmatic activity that began at ca. 43 Ma and lasted for at least 13 Myr (Figure 4). This period is interpreted as corresponding to batholith emplacement. In addition, these zircon U-Pb results suggest a broad NE-SW decreasing age gradient trend from the Middle Eocene (ca. 43 Ma) to the Lower Oligocene (ca. 30 Ma).

In addition to the high-temperature geochronometers (zircon and titanite), apatite was also analyzed in samples NE-01 (Necker Island), VG-01 (VG Island), CO-01 (Copper Island), and SA-01 (Salt Island). Within the margins of error, all the apatite ages are indistinguishable and span from 37.1 ± 1.7 Ma (Copper Island) to 35.1 ± 2.1 Ma (VG Island). Still within analytical uncertainties, these ages are younger or similar to those provided by co-existing zircons, suggesting that these apparent ages reflect cooling down to apatite U-Pb closure temperature. Cox et al. (1977), using the K-Ar method on biotite and hornblende, dated a quartz-diorite from VG Island and obtained apparent ages of 36.3 ± 0.9 and 34.2 ± 1.6 Ma, respectively. Apatite has a closure temperature in the range of 450–550°C, which is close to that of the K-Ar geochronometer in amphibole (Cherniak, 2000; Grove & Harrison, 1996; Harrison, 1981; Villa, 1998). Given the similarity between the U-Pb apatite ages and the K-Ar results of Cox et al. (1977), we interpret that apatite recorded the cooling of the plutons below ~500°C. Notably,

Figure 9. Initial Nd-Sr-Hf isotope correlation diagrams for the samples from British Virgin Islands. (a) $^{143}Nd/^{144}Nd$ ratios versus $^{87}Sr/^{86}Sr$ ratios diagram and (b) $^{176}Hf/^{177}Hf$ ratios versus $^{143}Nd/^{144}Nd$ ratios diagram. Reported for comparison: Mid-Oceanic Ridge Basalt (MORB) (gray) and island arc basalt (yellow) from Georoc database http://georoc.mpch-mainz.gwdg.de/georoc/; global pelagic sediments (dark blue) (Ben Othman et al., 1989; Plank & Langmuir, 1998; Vervoort et al., 2011); Antilles sediment composition (light blue) estimated from sediments of boreholes "Leg DSDP 78 site 144" and "Leg DSDP 78 site 543" from Carpentier et al. (2008); Depleted MORB Mantle (Workman & Hart, 2005), EM1 and EM2 (Enriched Mantle Type-1 and Type-2; Hart, 1984). NHRL: Northern Hemisphere Reference Line (Hart, 1984).

10.1029/2024GC012057

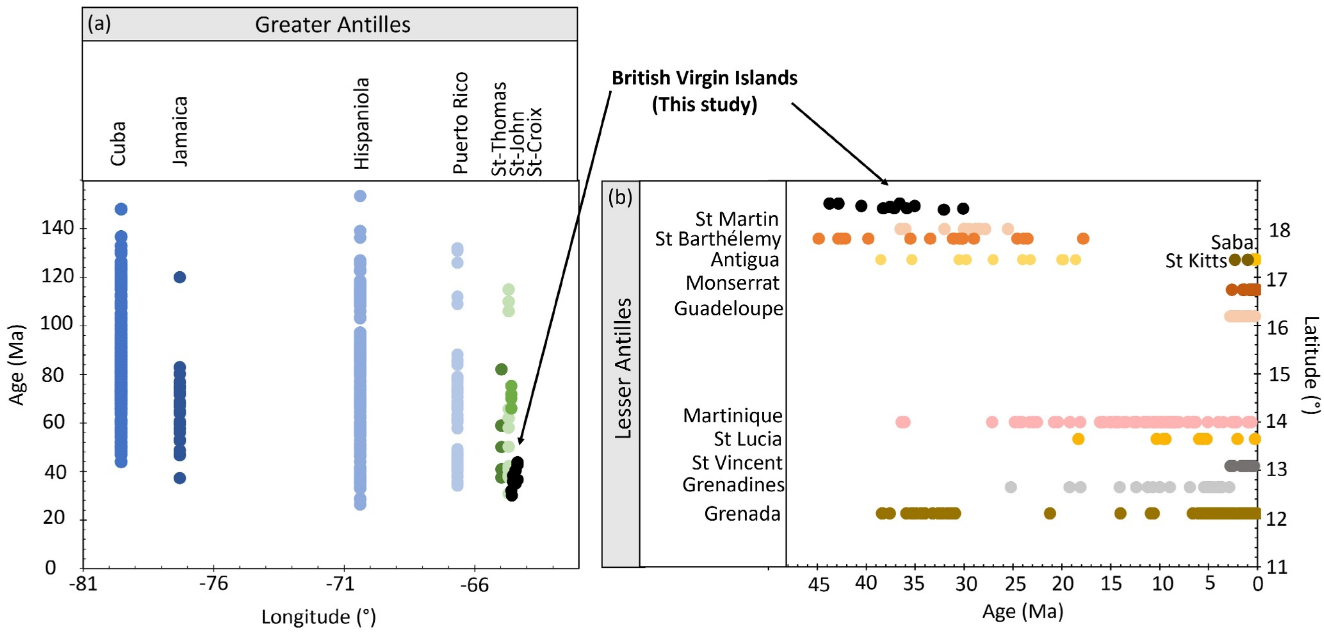

Figure 11. Distribution of the U-Pb ages obtained in this study for the British Virgin Islands (black dots) relative to their longitude (a) and their latitude (b). Are reported for comparison geochronological ages (U-Pb, Ar-Ar, and K-Ar) from the literature for the Greater Antilles (a): Cuba, Jamaica, Hispaniola, Puerto Rico and the American Virgin Islands (St-Croix, St-John, St Thomas) (see Hu et al., 2022, for references; Härtel et al., 2024) and for the Lesser Antilles (b): St Martin (Nagle et al., 1976; Noury et al., 2021), St-Barthelemy (Bosch et al., 2022; Legendre et al., 2018; Nagle et al., 1976), Antigua (Montheil, Philippon, Cornée, et al., 2023; Nagle et al., 1976), Saba (Defant et al., 2001), St Kitts (Baker, 1984), Montserrat (K. Brown & Davidson, 2008; Harford et al., 2002; Hatter et al., 2018), Guadeloupe (Briden et al., 1979; M. C. Brown et al., 2013; Favier et al., 2019; Verati et al., 2014), Martinique (Germa et al., 2011; Nagle et al., 1976); St Lucia (Briden et al., 1979); St Vincent (Briden et al., 1979); Grenadines (Briden et al., 1979; Speed et al., 1993) and Granada (Briden et al., 1979; Rojas-Agramonte et al., 2017; White et al., 2017).

the younger magmatic activity recorded by samples from the Peter and Norman Islands (ca. 30–32 Ma) did not reset the U-Pb system of the apatite from the northern islands. This observation is consistent with a southwestward migration of magmatic activity along the BVI archipelago.

The BVI are located between the Greater and the Lesser Antilles arcs and are separated from the Lesser Antilles by the Anegada Trough (Figure 1a). A compilation of absolute ages of the Greater Antilles islands (Härtel et al., 2024; Hu et al., 2022), including Cuba, Hispaniola, Jamaica, Puerto Rico and the Virgin Islands, indicates that the age distribution ranges from the Jurassic (ca. 155 Ma) to the Miocene (ca. 30 Ma) with most ages falling within the Cretaceous to Oligocene range (Figure 11). When focusing exclusively on arc magmatism and considering only U-Pb and Ar-Ar ages—regarded as the most reliable for determining crystallization ages—the age spectrum narrows to a range extending from the Cretaceous (133 Ma) to the Oligocene (30 Ma). Notably, within this range, there is a NW-SE decreasing age gradient from Cuba to the Virgin Islands. Indeed, Cuba and Hispaniola show close to similar age distributions, with three main peaks of magmatic activity at ca. 125–110 Ma, ca. 95–75 Ma and ca. 60–45 Ma. For Puerto Rico, only the peaks at ca. 95–75 and 60–45 Ma are identified, whereas the Virgin Islands show even younger ages, ranging from 45 to 30 Ma. Taken together, it is striking that magmatic events occurring between the Middle Eocene (i.e., <40 Ma) and the Oligocene (i.e., 30 Ma) are only detected exclusively in the Virgin Islands. This suggests a possible connection between the BVI and the other islands in the Greater Antilles arc, namely Cuba, Hispaniola and Puerto Rico. The latter appear, indeed, to have completed their magmatic evolution in the Middle Eocene, whereas the onset of magmatic activity started at that time in the BVI and ended during the Oligocene. This decreasing age gradient reflects the progressive suturing of the subduction zone and the accretion of the Cuban and Hispaniola portions of the Great Caribbean arc to the North American plate, while the plate boundary jumped along the Cayman trough.

Located South of the Anegada Trough, the Lesser Antilles arc is associated with the subduction of the north and south American plates beneath the Caribbean plate. It displays significantly more recent ages compared with the Greater Antilles. In its northern section (north of Martinique Island), the Lesser Antilles arc separates into two distinct branches, one extinct and one active (Figure 1a). In the northern part of the extinct arc, the islands of St.

Barthelemy and St. Martin yield magmatic ages ranging from ca. 42 Ma to ca. 20 Ma (Bosch et al., 2022; Legendre et al., 2018; Noury et al., 2021), which overlap entirely with the range defined for the magmatic activity in the BVI (this study), but pursued until ca. 20 Ma (Figure 11). In contrast, the active portion of the arc is significantly younger than the BVI, with magmatic activity beginning at ca. 20 Ma on St. Lucia and Martinique. This region shows more pronounced activity since the last ~5 Myr in St. Lucia, Martinique, Guadeloupe, Montserrat and the southern islands (Figures 1 and 11).

The chronology of magmatic activity in the Greater and Lesser Antilles arcs reveals a continuous trend of decreasing ages, generally progressing southeastward, from the Greater Antilles arc to the Lesser Antilles arc (Figure 11). The BVI, situated on the Puerto Rico Virgin Islands microplate, are part of the Greater Antilles arc and occupy an intermediate geographical position between the two arcs. The ages of the BVI partly overlap with those of the southern segment of the Greater Antilles arc and yield similar ages of the northern segment of the extinct Lesser Antilles arc. The magmatic activity in the BVI can thus be considered as a transitional segment between the Greater and the Lesser Antilles arcs.

5.2. Source Components and Geodynamical Context

All geochemical proxies (major and trace elements, Sr-Nd-Pb-Hf isotopes) used in this study consistently support the conclusion that the genesis of the BVI samples is associated with an oceanic subduction environment. Major element contents indicate a magmatic series with a calc-alkaline affinity, typical of magmas generated in an oceanic subduction zone. There is no significant evidence of detrital components typical of continental inputs, such as a pronounced increase in $^{207}Pb/^{204}Pb$ or $^{87}Sr/^{86}Sr$ ratios (Figures 8a and 9a). Trace element data also highlight typical subduction markers including a pronounced enrichment in LILEs (Cs, Rb, Ba, Sr), alongside a depletion in HFSE, as evidenced by negative anomalies in Nb-Ta, Zr-Hf and, to a lesser extent, Ti (Figure 7b). Finally, all the isotopic systems used in this study align with rocks formed within an oceanic arc domain (Figures 8 and 9).

Various components contribute, to different degrees, to the composition of island arc magmas. These include the mantle wedge and slab-derived materials from the subducted oceanic crust and the sediments on top of it. The REE patterns reveal that most of the BVI samples, except for those from VG and Peter Islands, exhibit minimal variations. This similarity suggests a relatively homogeneous mantle source characterized by a composition close to the N-MORB mantle average (Arevalo & McDonough, 2010). This is corroborated by the Hf isotopes, which define a relatively limited variation of εHf_i ($+12.7 < \varepsilon Hf_i < +14$; Table S7 in Supporting Information S1) except for the Peter Island rocks showing slightly lower εHf. These values are in good agreement with the compositions commonly accepted for the Atlantic MORB domain (Andres et al., 2002). Moreover, this suggests moreover that the Hf isotopes have not been significantly modified during interactions with the slab component. This also supports the idea that the mantle wedge below the BVI has likely remained relatively unchanged in composition over the estimated 13 Myr of arc magmatism recorded in the archipelago.

In Figure 7b, the extended trace element patterns are compared to the average MORB (Arevalo & McDonough, 2010) as a first approximation of an unmodified mantle wedge composition. This comparison helps distinguish between proxies coming from the slab and those originating from the mantle wedge. Depending on the thermal conditions, the sediments overlying the oceanic crust at the top of the subducting slab can contribute to magma generation through dehydration or melting processes. Most of the BVI samples show moderate to high enrichment in mobile elements such as Cs, Rb, Ba, Th, U, La, Pb, and Sr relative to the MORB composition. All the samples, excluding the volcanic sample from Necker Island, show strong negative Nb-Ta and Zr-Hf anomalies. During subduction processes and associated slab-mantle wedge interactions, it is possible, based on trace element contents, to distinguish a contribution from a subduction component dominated either by slab dehydration (aqueous fluids) or by sediment melting. LILEs preferentially migrate into the fluid phase and thus become incorporated into the new magmas formed. Conversely, HFSEs are not easily mobilized from the slab during dehydration processes (Tatsumi et al., 1986) and thus only contribute to the new magma formed through melting processes, either as sediment melts or bulk sediments (Cassidy et al., 2012; Plank, 2005). The influence of slab-derived fluids can also be identified by the increase in mobile elements/REE ratios, as expressed by the Ba/La and Pb/Ce ratios. For the BVI samples, Ba/La and Pb/Ce ratios range from 15 to 173 and from 0.1 to 1.4, respectively, and are significantly distinct from the average MORB values (i.e., Ba/La = 6.8 and Pb/Ce = 0.05; after Arevalo & McDonough, 2010). The observed enrichment in LILEs are thus interpreted as reflecting the

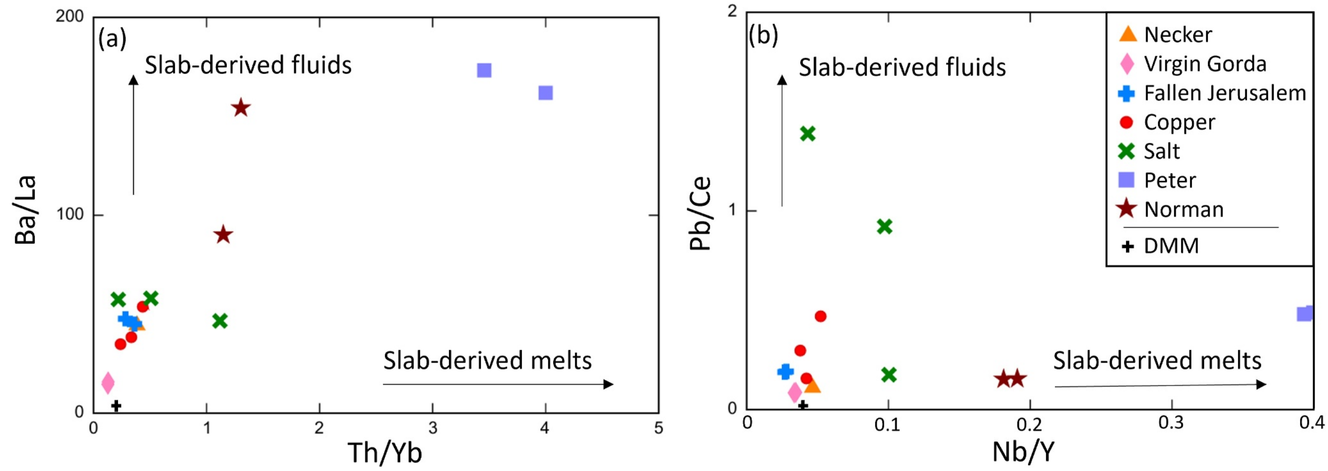

Figure 12. Diagrams (a) Ba/La versus Th/Yb and (b) Pb/Ce versus Nb/Y for the British Virgin Islands samples. Arrows indicate slab-derived fluids and melts. The DMM value is indicated by a dark cross (Workman & Hart, 2005).

involvement of slab-derived fluids. Additionally, the sediment melt contribution can be identified using a ratio between a reputed immobile element and a REE or between two immobile elements, for example, using the Th/Yb and Nb/Y ratios. In the Ba/La versus Th/Yb and Pb/Ce versus Nb/Y diagrams (Figures 12a and 12b) it is possible to distinguish between fluids and/or slab-derived melt contributions. Samples from the BVI show similar behaviors in both diagrams. The samples from FJ, Copper and one out of the three samples from Salt Island are characterized by varying degrees of enrichment in Ba/La and Pb/Ce without notable increases in Th/Yb or Nb/Y. This behavior suggests the involvement of slab fluids without significant slab melt participation. In contrast, the samples from Peter and Norman Islands along with two out of three samples from Salt Island show moderate to high increases in Ba/La and Pb/Ce ratios and an increase inthe Th/Yb and Nb/Y ratios. This is interpreted as evidence of slab-derived melt in the southwestern islands of the archipelago, superimposed on fluid inputs derived from slab dehydration processes. Interestingly, the presence of a slab-derived melt component is mainly detected in samples from Peter and Norman Islands, which yielded ages younger than the Eocene.

To roughly estimate the percentage contribution of the slab-derived component in the BVI samples, isotopic proxies can be modeled using simple binary mixing. Different considerations have been taken into account while performing this modeling: (a) only bulk solid-solid mixing calculations were considered; (b) the mantle wedge component has been modeled using the average Atlantic MORB value of Workman and Hart (2005); (c) the slab-derived sediment end-members were represented by the most enriched and most depleted compositions of two sediment sites (DSDP 144 and 543) drilled off the Lesser Antilles island arc (Carpentier et al., 2008); (d) considering that the sediment component contribute through fluid or melt the percentage calculated in the modeling is assumed to correspond to the maximum values of the mixing; (e) the oceanic crust underlying the sediments of the slab has not been taken into account considering that it is probably close to the average Atlantic MORB composition. The result of this modeling is presented in Figure 13. The BVI samples are located close to the mixing lines indicative of mixing between the mantle component and the less radiogenic poles of the DSDP 144 and DSDP 543 sediments. The estimated percentage for the contribution of sediments necessary to explain the Pb and Nd isotope signatures of the BVI samples remains low, that is, less than 1.8%. Specifically, the samples from Norman, Peter, and Cooper (CO-01) show the highest sediment contributions, ranging from 0.7% to 1.8%, depending on the sedimentary pole considered. The samples from the other islands show a lower sediment involvement (<0.7%). These results are consistent with previous modeling for the northern arc of the Lesser Antilles, where the sedimentary contributions involved in magma genesis are estimated to be lower than 2% (Bosch et al., 2022; Carpentier et al., 2008; Cassidy et al., 2012; Davidson, 1987; Zellmer et al., 2003). This low percentage of sediment contribution in the BVI samples helps to explain why the εHf signature of these samples shows typical mantle wedge characteristics (e.g., Andres et al., 2002). More interestingly, samples from Norman and Peter Islands, the youngest samples in this study, yield the most pronounced sedimentary signatures (Figures 12a and 12b). This increase in sediment contribution to the magma source may be attributed to several geodynamic factors, such as an increased thickness of the subducted sediments, a geographical change in the

10.1029/2024GC012057

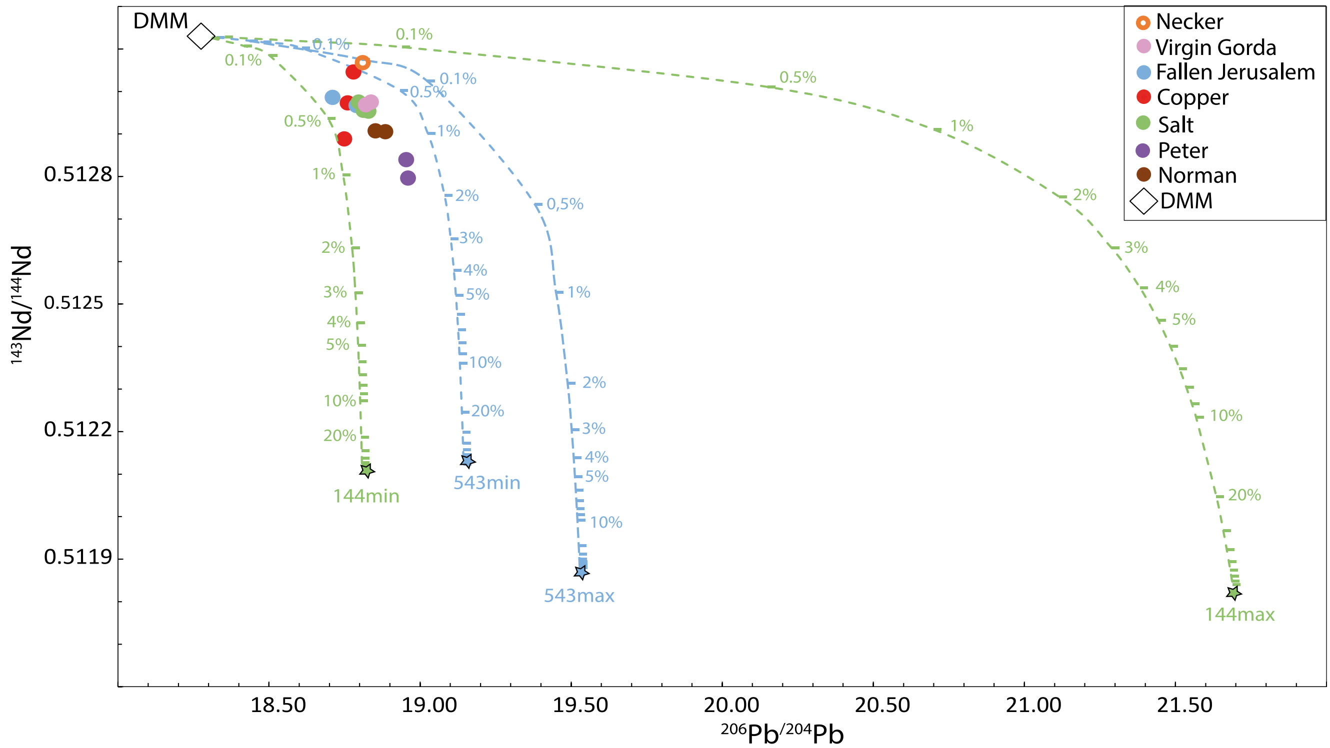

Figure 13. Initial $^{143}Nd/^{144}Nd$ versus $^{206}Pb/^{204}Pb$ diagram for the British Virgin Islands samples. The four mixing curves correspond to the sedimentary end-members, that is, "144 min" and "144 max" and "543 min" and "543 max", which are the least and most enriched poles for the "Leg DSDP 78 Site 144" and "Leg DSDP 78 Site 543" (Carpentier et al., 2008). The mantle pole corresponds to the DMM (Workman & Hart, 2005). The concentration and isotopic ratios assumed for depleted mantle are the following: Pb = 0.018 ppm, Nd = 0.581 ppm and $^{206}Pb/^{204}Pb = 18.275$, $^{143}Nd/^{144}Nd = 0.51313$ corresponding to average DMM values after Workman and Hart (2005). Numbered ticks along the mixing lines correspond to the percentage of sediment in the mixture. The mixing models presented in this figure assume a uniform composition of the endmembers, which is undoubtedly an oversimplification; thus, the values should be considered as indicative only.

composition of the subducted sedimentary pile, an increase in subduction velocity, enhanced tectonic erosion at the plate interface, or a drastic change in the tectonic regime. These scenarios will be discussed in more detail in Section 5.3.

Lastly, the study of a continuous intra-oceanic paleo-arc section (Dhuime et al., 2009) revealed a progressive evolution of the trace element patterns from the N-MORB-type corresponding to a high proportion of the mantle-wedge to the calc-alkaline-type, including a significant proportion of the slab component. These changes in trace element distribution were interpreted as reflecting different stages of the subduction activity, that is, from the beginning to a more mature regime. Similarly, the VG gabbros could possibly be interpreted as the witnesses subduction initiation, while the Peter Island quartz-monzonites could indeed correspond to a more mature subduction regime.

To compare the geochemical composition of the BVI with the overall Antilles islands arcs the Δ7/4Pb and Δ8/4Pb values were reported as a function of the $^{206}Pb/^{204}Pb$ ratio (Figure 14). Since Δ7/4Pb and Δ8/4Pb values represent the deviation of the $^{207}Pb/^{204}Pb$ and $^{208}Pb/^{204}Pb$ ratios from the NHRL at a given $^{206}Pb/^{204}Pb$ ratio (Hart, 1984), they reflect the proportions of the non-mantle components, and hence of subducted sediments, involved in the magma genesis. The available data for the Lesser Antilles arc define distinct domains for the various islands but consistently exhibit more radiogenic $^{206}Pb/^{204}Pb$ ratios than the domains defined for the Greater Antilles arc islands, namely Cuba, Hispaniola and Puerto Rico (Figure 14). Overall, the data set tends to define a distribution gradient from the Greater Antilles to the Lesser Antilles, with the extinct Lesser Antilles arc positioned in between. When arranged from the least to the most radiogenic $^{206}Pb/^{204}Pb$ ratios, the succession of the different islands begins with Hispaniola, Cuba and Puerto Rico followed by St. Martin, St. Barthélemy, Montserrat, St. Kitts, Dominica and Les Saintes and ends with Martinique in the Lesser Antilles. The BVI occupy a relatively large domain that partially overlaps with the fields defined by the northern section of the extinct Lesser Antilles arc, specifically the islands of St. Martin and St. Barthélemy (Figure 14). Values obtained for the

10.1029/2024GC012057

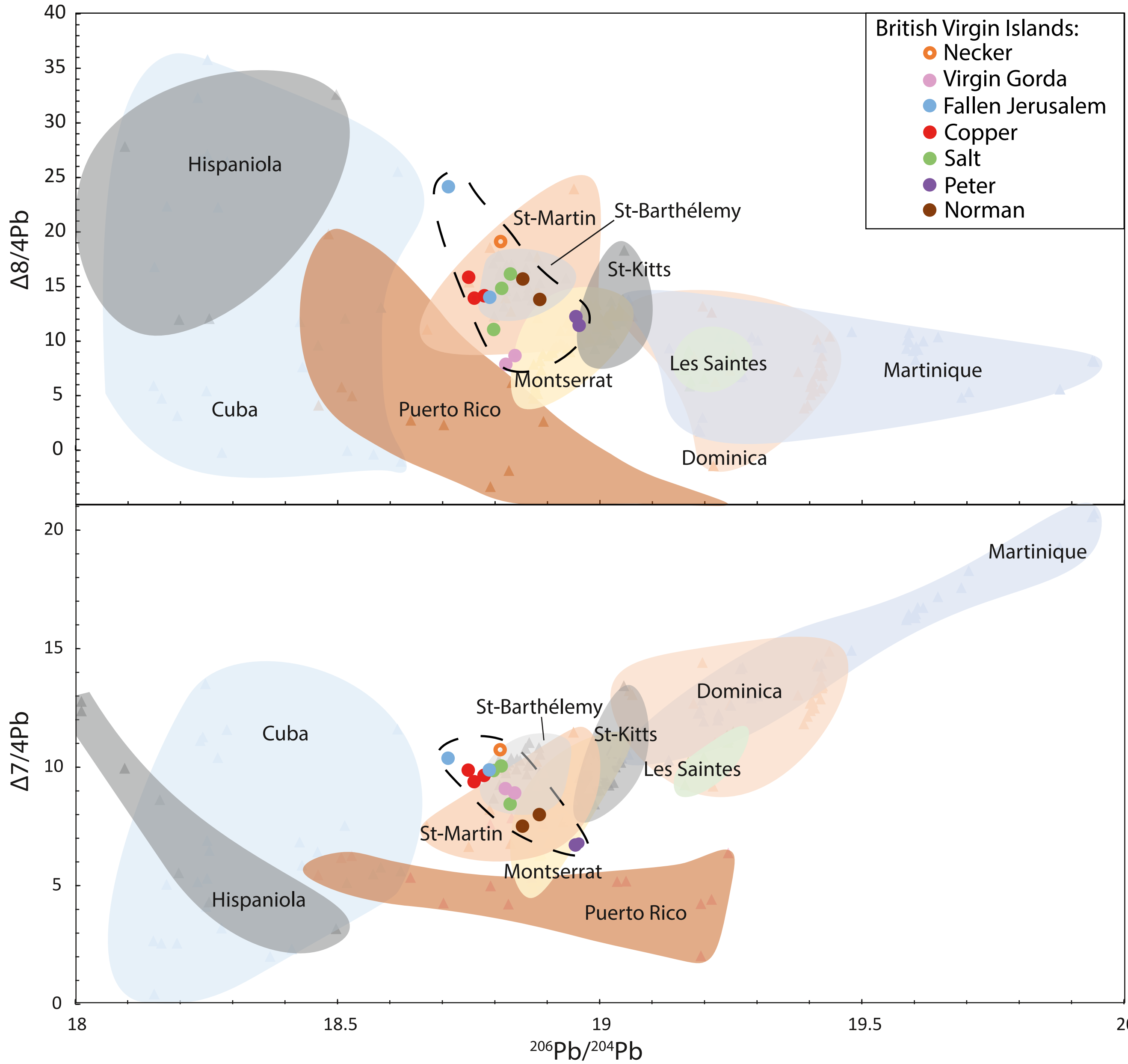

Figure 14. Diagram of the initial $^{206}Pb/^{204}Pb$ ratio for the British Virgin Islands versus (a) Δ7/4Pb and (b) Δ8/4Pb compared to other islands of the Antilles arc. Δ7/4 and Δ8/4 were calculated according to the equation defined by Hart (1984): $\Delta 7/4 = (^{207}Pb/^{204}Pb)_{sample} - (^{207}Pb/^{204}Pb)_{NHRL} * 100$ and $\Delta 8/4 = (^{208}Pb/^{204}Pb)_{sample} - (^{208}Pb/^{204}Pb)_{NHRL} * 100$. The geochemical domains of the Greater and Lesser Antilles are taken from a compilation of the literature: Cuba (Marchesi et al., 2007); Hispaniola (Lapierre et al., 1999); Puerto Rico (Jolly et al., 1998); St Martin (Davidson et al., 1993); St-Barthélemy (Bosch et al., 2022); St. Kitts (Toothill et al., 2007); Montserrat (Cassidy et al., 2012); Dominica (Lindsay et al., 2005); Martinique (Labanieh et al., 2010) and les Saintes (Bosch et al., 2022).

BVI plot in an intermediate position between the domains defined for the Greater Antilles, particularly Cuba, and the central to southern Lesser Antilles arc islands belonging to the active arc (i.e., Montserrat, St. Kitts, les Saintes, Dominica and Martinique). Based on the geochronological data and geochemical proxies obtained in this study, the BVI correspond to a transition zone between the Greater Antilles and the Lesser Antilles magmatic arcs.

5.3. Geodynamic Evolution of the British Virgin Islands Within the Caribbean Arc

Geochronological and thermobarometrical data from this study reveal that the oldest plutons in the BVI, located in the northeast of the archipelago, were emplaced at a lower depth of ~5.5 km, while the youngest plutons in the southwest, which were emplaced at a deeper depth of ∼15 km. This shows that the upward movement of rocks relative to the surface (i.e., the rock exhumation) must have been greater and faster in the southwest compared to the northeast of the BVI because at present day these plutons are at the same structural level. Since there are no known large NW-SE trending and NE-dipping normal faults to explain this differential exhumation, we propose that the BVI archipelago belongs to a single crustal block that underwent a net northeastward tilting. This tilting likely occurred before the Upper Oligocene—Early Miocene, as suggested by low temperature thermochronology data, which indicate that all plutons were at similar depths around 24–21 Ma (Román et al., 2021). This local observation correlates with the regional west-east exhumation gradient observed from Puerto Rico to the Virgin Islands (Román et al., 2021). To the south of Anegada, the island of St Martin yields similar results with a rapid exhumation from 28 to 24 Ma, which is consistent with the regional exhumation gradient (Noury et al., 2021).

Our study demonstrates that the BVI magmatism was active from ca. 43 to 30 Ma and that the rocks from the different islands share common ages and geochemical features with the extinct arc of the Lesser Antilles currently exposed in the islands of Antigua, St Barthélemy and Saint Martin (Bosch et al., 2022; Legendre et al., 2018; Montheil, Philippon, Cornée, et al., 2023; Noury et al., 2021). These results thus suggest that the Puerto Rico—Virgin Islands and the northern Lesser Antilles belonged to the same tectonic block during the Eocene. Recent tectonic reconstructions show that the Puerto Rico-Virgin Islands and the northern Lesser Antilles belonged to a single tectonic block (GraNoLA), that rotated ∼40° counterclockwise. The GrANoLA block moved laterally along the subduction zone over ∼500 km since the mid-Eocene as a forearc sliver (Montheil, Philippon, Münch, et al., 2023). When restored from their rotation, the BVI plutons were emplaced along an east-west trench perpendicular direction (Figure 15). In this context, a slight horizontalization of the subducting slab angle during the Eocene-Oligocene might explain the apparent NE to SW gradient of decreasing crystallization ages evidenced in this study (Figure 15a).

After that, the cessation of the BVI magmatic activity, assumed at around ca. 30 Ma, may be attributed to a shift in the BVI' crustal block position relative to the slab during forearc sliver motion, and to interaction with the Bahamas bank, which would thus lead to subduction end (Figure 15b). Puerto Rico likely initiated its motion toward the highly oblique portion of the subduction zone first, followed by a similar movement of BVI. This block motion along the plate boundary may also account for the increasing amount of slab-derived sediment detected in the southwestern BVI, that is, the Norman and Peter Islands, and the concomitant increasing contribution of sedimentary melts. The involvement of these later types of slab-derived components, that is, sediment melts, may have been facilitated by the highly oblique nature of the subduction zone, which could have triggered an increase in the slab's temperature as the mantle wedge migrated, just before the magmatic activity ceased in the region. Recent 3-D numerical modeling has shown that with increasing obliquity, the trench-parallel component of the velocity consequently increases and the temperature variation reaches 200°C along-strike (Plunder et al., 2018). The continuous transition observed between the Puerto Rico—Virgin Islands and the northern Lesser Antilles arc has major implications for the geodynamic models proposed for the evolution of the eastern Caribbean subduction zone's evolution. This continuity suggests that there was no subduction jump, as previously proposed (Bouysse & Westercamp, 1990; Conrad et al., 2024), but rather a single continuous slab involved in both the BVI and northern Lesser Antilles magmatism.

6. Conclusion

The BVI, currently located in the Puerto Rico—Virgin Islands block, record a magmatic activity spanning 13 Myr, from Middle Eocene (ca. 43 Ma) to Oligocene (ca. 30 Ma). The geochemical characteristics of the rocks from the different islands are typical of calk-alkaline magmas formed in a subduction zone setting with involvement of a mantle-wedge with a composition close to that of the Atlantic mantle MORB and a low slab-derived sedimentary (<1.7%) contribution characterized by a composition compatible with the least radiogenic sediments drilled in the DSDP 144 and 543 (Carpentier et al., 2008). A noticeable change in the sedimentary supply is registered for the Oligocene islands of Norman and Peter located at the southwestern extremity of the archipelago. Temporal constraints and geochemical characteristics display strong similarities with the islands from the northern extinct Lesser Antilles arc. The new BVI ages and geochemical proxies thus demonstrate that there is a temporal and geographical continuous transition between the Greater and the Lesser Antilles arcs. The BVI and northern Lesser Antilles record this transitional period, which corresponds to a period of regional geodynamic change with relative motion between the North American and Caribbean plates. During the Eocene, the Puerto Rico—Virgin Islands and the northern Antilles were part of the same tectonic block. The change in the

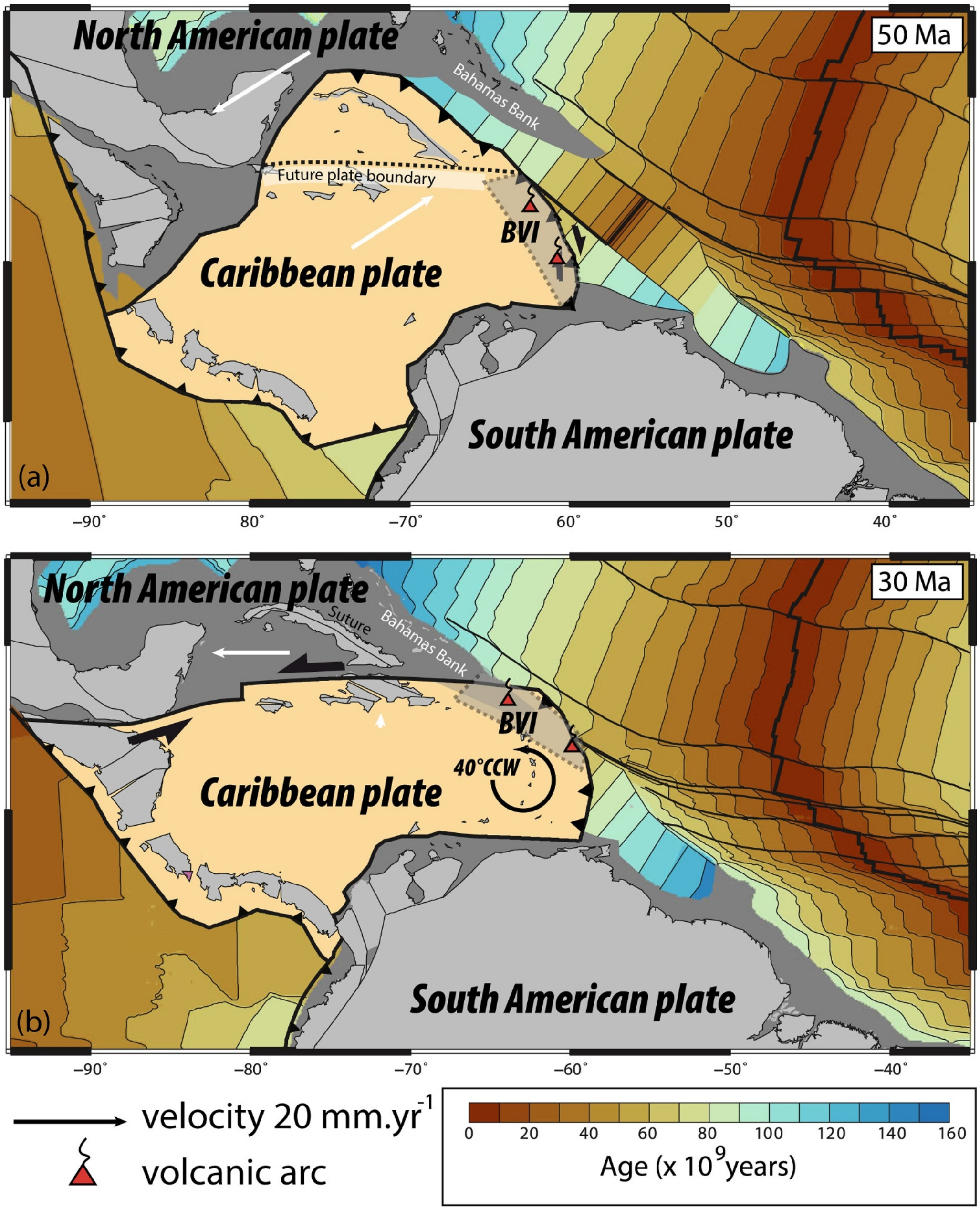

Figure 15. Reconstruction of the geodynamic evolution of the Caribbean, modified from Müller et al. (2016) and Braszus et al. (2021). The age of the oceanic lithosphere is represented by a color scale. The continental lithosphere is shown in gray with the current coastlines in light gray. The red triangles represent the active magmatism of the Antilles arc. (a) 50 Ma Subduction of the North American plate beneath the northern segment of the Greater Antilles. Subduction of the Atlantic oceanic lithosphere to the east of the Caribbean plate. (b) 30 Ma The northern segment of the Greater Antilles becomes inactive after collision with the Bahamas Bank, creating a new boundary for the North Caribbean plate. Subduction of the thinned continental crust of the Bahamas Bank at the level of the Virgin Islands and the northern islands of the Lesser Antilles. BVI: British Virgin Islands; ccw: counterclockwise.

nature of the sedimentary input from fluid to melt + fluid in the BVI magmatism, assumed to have occurred just before 30 Ma, may be explained by a change in the BVI' location relative to the slab position during the motion of the forearc sliver and the interaction with the Bahamas bank, which would thus have acted as a blocker of subduction. The cessation of magmatism may be explained by the westward motion of the Puerto Rico—Virgin

Islands microblock. This model challenges previous tectonics models and suggests that a single, uninterrupted subduction zone was responsible for magmatism in both the BVI and northern Lesser Antilles.

Data Availability Statement

The geochemical dataset (Tables S1–S7 in Supporting Information S1) will be made publicly available in the Zenodo data repository via Bosc et al. (2025).

Acknowledgments
We are grateful to Léa Causse and Lucie Koeller for their help during ICP-MS and ICP-OES analyses at the AETE-ISO facility service from Montpellier University. We also thank C. Nevado and D. Delmas for thin and thick section preparation and to F. Fernandez for SEM photographs. N. Salazar from the Unidad de Microanálisis of the Instituto de Geofísica Unidad Morelia, UNAM is thanked for her help with EPMA analyses. J.M. Dautria is acknowledged for his help during thin-section examination. We are grateful to Lisard Torró, an anonymous reviewer and the associated editor Yamirka Rojas-Agramonte for their helpful and constructive comments on the manuscript. Fieldwork and rock sampling were funded by research funding of Antilles University and ANR SUBUTTEC ANR-23-CE01-0028. Geochemical analyses (major, trace elements and isotopes), including geochronology, were supported by TELLUS-SYSTER (2021–2022) research funding (D.B). This work is part of the Master Thesis work of N.B.

References

Ague, J. J. (1997). Thermodynamic calculation of emplacement pressures for batholithic rocks, California: Implications for the aluminum-in-hornblende barometer. *Geology*, *25*(6), 563–566. https://doi.org/10.1130/0091-7613(1997)025<0563:tcoepf>2.3.co;2

Allen, R. W., Collier, J. S., Stewart, A. G., Henstock, T., Goes, S., Rietbrock, A., & the VoiLA Team. (2019). The role of arc migration in the development of the Lesser Antilles: A new tectonic model for the Cenozoic evolution of the eastern Caribbean. *Geology*, *47*(9), 891–895. https://doi.org/10.1130/G46708.1

Andres, M., Blichert-Toft, J., & Schilling, J. (2002). Hafnium isotopes in basalts from the southern Mid-Atlantic Ridge from 40°S to 55°S: Discovery and Shona plume–ridge interactions and the role of recycled sediments. *Geochemistry, Geophysics, Geosystems*, *3*(10), 1–25. https://doi.org/10.1029/2002GC000324

Arevalo, R., & McDonough, W. F. (2010). Chemical variations and regional diversity observed in MORB. *Chemical Geology*, *271*(1–2), 70–85. https://doi.org/10.1016/j.chemgeo.2009.12.013

Atlas, Z. D., Germa, A., Boss, B., Meireles, O., Ward, A., & Ryan, J. G. (2022). Variable element enrichment sources and contributions to volcanic rocks along the Lesser Antilles Island Arc. *Frontiers in Earth Science*, *10*, 782179. https://doi.org/10.3389/feart.2022.782179

Audemard, F. A. (2009). Key issues on the post-Mesozoic southern Caribbean Plate boundary. *Geological Society*, *328*(1), 569–586. https://doi.org/10.1144/SP328.23

Baker, P. E. (1984). Geochemical evolution of St Kitts and Montserrat, LesserAntilles. *Journal of the Geological Society*, *141*(3), 410–411. https://doi.org/10.1144/gsjgs.141.3.0401

Ben Othman, D., White, W. M., & Patchett, J. (1989). The geochemistry of marine sediments, Island arc magma genesis, and crust-mantle recycling. *Earth and Planetary Science Letters*, *94*(1–2), 1–21. https://doi.org/10.1016/0012-821X(89)90079-4

Blichert-Toft, J. (2008). The Hf isotopic composition of zircon reference material 91500. *Chemical Geology*, *253*(3–4), 252–257. https://doi.org/10.1016/j.chemgeo.2008.05.014

Bosc, N., Bosch, D., Noury, M., Bruguier, O., Montheil, L., van Hinsbergen, D. J. J., et al. (2025). Tracking the Caribbean magmatic evolution: The British Virgin Islands as a transition between the Greater and Lesser Antilles arcs [Dataset]. *Zenodo*. https://doi.org/10.5281/zenodo.15077476

Bosch, D., Zami, F., Philippon, M., Lebrun, J., Münch, P., Cornée, J., et al. (2022). Evolution of the Northern part of the Lesser Antilles arc—Geochemical constraints from St. Barthélemy Island lavas. *Geochemistry, Geophysics, Geosystems*, *23*(10), e2022GC010482. https://doi.org/10.1029/2022GC010482

Boschman, L. M., Van Der Wiel, E., Flores, K. E., Langereis, C. G., & Van Hinsbergen, D. J. J. (2019). The Caribbean and Farallon plates connected: Constraints from stratigraphy and paleomagnetism of the Nicoya Peninsula, Costa Rica. *Journal of Geophysical Research: Solid Earth*, *124*(7), 6243–6266. https://doi.org/10.1029/2018JB016369

Boschman, L. M., Van Hinsbergen, D. J. J., Torsvik, T. H., Spakman, W., & Pindell, J. L. (2014). Kinematic reconstruction of the Caribbean region since the early Jurassic. *Earth-Science Reviews*, *138*, 102–136. https://doi.org/10.1016/j.earscirev.2014.08.007

Bouvier, A., Vervoort, J. D., & Patchett, P. J. (2008). The Lu–Hf and Sm–Nd isotopic composition of CHUR: Constraints from unequilibrated chondrites and implications for the bulk composition of terrestrial planets. *Earth and Planetary Science Letters*, *273*(1–2), 48–57. https://doi.org/10.1016/j.epsl.2008.06.010

Bouysse, P., & Westercamp, D. (1990). Subduction of Atlantic aseismic ridges and Late Cenozoic evolution of the Lesser Antilles island arc. *Tectonophysics*, *175*(4), 349–380. https://doi.org/10.1016/0040-1951(90)90180-G

Bralower, T. J., & Iturralde-Vinent, M. A. (1997). Micropaleontological dating of the collision between the North American plate and the greater Antilles arc in western Cuba. *PALAIOS*, *12*(2), 133. https://doi.org/10.2307/3515303

Braszus, B., Goes, S., Allen, R., Rietbrock, A., Collier, J., Harmon, N., et al. (2021). Subduction history of the Caribbean from upper-mantle seismic imaging and plate reconstruction. *Nature Communications*, *12*(1), 4211. https://doi.org/10.1038/s41467-021-24413-0

Briden, J. C., Rex, D. C., Faller, A. M., & Tomblin, J. F. (1979). K-Ar geochronology and paleomagnetism of volcanic rocks in the Lesser Antilles Island Arc. *Royal Society*, *291*(1383), 485–528. Retrieved from https://www.jstor.org/stable/75166

Brown, K., & Davidson, C. (2008). $^{40}Ar/^{39}Ar$ geochronology of the Silver Hills andesite, Montserrat, West Indies. BA Sr. Integr. Exerc. Carlton College, Northfield, Minnesota.

Brown, M. C., Jicha, B. R., Singer, B. S., & Shaw, J. (2013). Snapshot of the Matuyama-Brunhes reversal process recorded in $^{40}Ar/^{39}Ar$-dated lavas from Guadeloupe, West Indies. *Geochemistry, Geophysics, Geosystems*, *14*(10), 4341–4350. https://doi.org/10.1002/ggge.20263

Bruguier, O., Caby, R., Bosch, D., Ouzegane, K., Deloule, E., Dhuime, B., et al. (2020). A case study of in situ analyses (major and trace elements, U-Pb geochronology and Hf-O isotopes) of a zircon megacryst: Implication for the evolution of the Egéré terrane (Central Hoggar, Tuareg Shield, Algeria). *Precambrian Research*, *351*, 105966. https://doi.org/10.1016/j.precamres.2020.105966

Burke, K. (1988). Tectonic evolution of the Caribbean. *Annual Review of Earth and Planetary Sciences*, *16*(1), 201–230. https://doi.org/10.1146/annurev.ea.16.050188.001221

Byrne, D. B., Suarez, G., & McCann, W. R. (1985). Muertos Trough subduction—Microplate tectonics in the northern Caribbean? *Nature*, *317*(6036), 420–421. https://doi.org/10.1038/317420a0

Carpentier, M., Chauvel, C., & Mattielli, N. (2008). Pb–Nd isotopic constraints on sedimentary input into the Lesser Antilles arc system. *Earth and Planetary Science Letters*, *272*(1–2), 199–211. https://doi.org/10.1016/j.epsl.2008.04.036

Cassidy, M., Taylor, R. N., Palmer, R. J., Cooper, R. J., Stenlake, C., & Trofimovs, J. (2012). Tracking the magmatic evolution of island arc volcanism: Insights from a high-precision Pb isotope record of Montserrat, Lesser Antilles. *Geochemistry, Geophysics, Geosystems*, *13*, 5Q05003. https://doi.org/10.1029/2012gc004064

Chauvel, C., & Blichert-Toft, J. (2001). A hafnium isotope and trace element perspective on melting of the depleted mantle. *Earth and Planetary Science Letters*, *190*(3–4), 137–151. https://doi.org/10.1016/s0012-821x(01)00379-x

Cherniak, D. J. (2000). Rare earth element diffusion in apatite. *Geochimica et Cosmochimica Acta*, *64*(22), 3871–3885. https://doi.org/10.1016/S0016-7037(00)00467-1

Chew, D. M., Sylvester, P. J., & Tubrett, M. N. (2011). U–Pb and Th–Pb dating of apatite by LA-ICPMS. *Chemical Geology*, *280*(1–2), 200–216. https://doi.org/10.1016/j.chemgeo.2010.11.010

Colmenares, L., & Zoback, M. D. (2003). Stress field and seismotectonics of northern South America. *Geology*, *31*(8), 721. https://doi.org/10.1130/G19409.1

Connelly, J. N., Ulfbeck, D. G., Thrane, K., Bizzarro, M., & Housh, T. (2006). A method for purifying Lu and Hf for analyses by MC-ICP-MS using TODGA resin. *Chemical Geology*, *233*(1–2), 126–136. https://doi.org/10.1016/j.chemgeo.2006.02.020

Conrad, E. M., Faccenna, C., Holt, A. F., & Becker, T. W. (2024). Tectonic reorganization of the Caribbean Plate system in the Paleogene Driven by Farallon slab Anchoring. *Geochemistry, Geophysics, Geosystems*, *25*(8), e2024GC011499. https://doi.org/10.1029/2024GC011499

Cornée, J.-J., Münch, P., Philippon, M., BouDagher-Fadel, M., Quillévéré, F., Melinte-Dobrinescu, M., et al. (2021). Lost islands in the northern lesser Antilles: Possible milestones in the Cenozoic dispersal of terrestrial organisms between south-America and the greater Antilles. *Earth-Science Reviews*, *217*, 103617. https://doi.org/10.1016/j.earscirev.2021.103617

Cox, D. P., Marvin, R. F., M'Gonigle, J. W., McIntyre, D. H., & Rogers, C. L. (1977). Potassium-Argon geochronology of some metamorphic, igneous, and hydrothermal events in Puerto Rico and the Virgin Islands. *U.S. Geological Survey Journal of Research*, *5*(6), 689–703.

Davidson, J. P. (1987). Crustal contamination versus subduction zone enrichment: Examples from the Lesser Antilles and implications for mantle source compositions of island arc volcanic rocks. *Geochimica et Cosmochimica Acta*, *51*(8), 2185–2198. https://doi.org/10.1016/0016-7037(87)90268-7

Davidson, J. P., Boghossian, N., & Wilson, M. (1993). The geochemistry of the igneous rock suite of St Martin, northern lesser Antilles. *Journal of Petrology*, *34*(5), 839–866. https://doi.org/10.1093/petrology/34.5.839

Defant, M. J., Sherman, S., Maury, R. C., Bellon, H., De Boer, J., Davidson, J., & Kepezhinskas, P. (2001). The geology, petrology, and petrogenesis of Saba island, lesser Antilles. *Journal of Volcanology and Geothermal Research*, *107*(1–3), 87–111. https://doi.org/10.1016/S0377-0273(00)00268-7

DeMets, C., Jansma, P. E., Mattioli, G. S., Dixon, T. H., Farina, F., Bilham, R., et al. (2000). GPS geodetic constraints on Caribbean-north America plate motion. *Geophysical Research Letters*, *27*(3), 437–440. https://doi.org/10.1029/1999GL005436

Dhuime, B., Bosch, D., Garrido, C. J., Bodinier, J. L., Bruguier, O., Hussain, S. S., & Dawood, H. (2009). Geochemical architecture of the lower-to middle-crustal section of a paleo-island arc (Kohistan Complex, Jijal–Kamila area, northern Pakistan): Implications for the evolution of an oceanic subduction zone. *Journal of Petrology*, *50*(3), 531–569. https://doi.org/10.1093/petrology/egp010

Favier, A., Lardeaux, J. M., Legendre, L., Verati, C., Philippon, M., Corsini, M., et al. (2019). Tectono-metamorphic evolution of shallow crustal levels within active volcanic arcs. Insights from the exhumed Basal Complex of Basse-Terre (Guadeloupe, French West Indies). *Bulletin de la Societe Geologique de France*, *190*(1), 10. https://doi.org/10.1051/bsgf/2019011

Ferry, J. M., & Watson, E. B. (2007). New thermodynamic models and revised calibrations for the Ti-in-zircon and Zr-in-rutile thermometers. *Contributions to Mineralogy and Petrology*, *154*(4), 429–437. https://doi.org/10.1007/s00410-007-0201-0

Germa, A., Quidelleur, X., Labanieh, S., Chauvel, C., & Lahitte, P. (2011). The volcanic evolution of Martinique Island: Insights from K–Ar dating into the Lesser Antilles arc migration since the Oligocene. *Journal of Volcanology and Geothermal Research*, *208*(3–4), 122–135. https://doi.org/10.1016/j.jvolgeores.2011.09.007

Gill, J. B. (1981). What is 'typical Calcalkaline Andesite'? In *Orogenic Andesites and plate tectonics* (Vol. 16, pp. 1–12). Springer. https://doi.org/10.1007/978-3-642-68012-0_1

Gordon, M. B., Mann, P., Cáceres, D., & Flores, R. (1997). Cenozoic tectonic history of the North America-Caribbean plate boundary zone in western Cuba. *Journal of Geophysical Research*, *102*(B5), 10055–10082. https://doi.org/10.1029/96JB03177

Grove, M., & Harrison, T. M. (1996). ^{40}Ar* diffusion in Fe-rich biotite. *American Mineralogist*, *81*(7–8), 940–951. https://doi.org/10.2138/am-1996-7-816

Hammarstrom, J. M., & Zen, E.-A. (1986). Aluminum in hornblende: An empirical igneous geobarometer. *American Mineralogist*, *71*, 1297–1313.

Harford, C. L., Pringle, M. S., Sparks, R. S. J., & Young, S. R. (2002). The volcanic evolution of Montserrat using 40Ar/39Ar geochronology. *Geological Society, London, Memoirs*, *21*(1), 93–113. https://doi.org/10.1144/GSL.MEM.2002.021.01.05

Harrison, T. M. (1981). Diffusion of Ar-40 in hornblende. *Contributions to Mineralogy and Petrology*, *78*(3), 324–331. https://doi.org/10.1007/bf00398927

Hart, S. R. (1984). A large-scale isotope anomaly in the Southern Hemisphere mantle. *Nature*, *309*(5971), 753–757. https://doi.org/10.1038/309753a0

Härtel, B. P., Frei, O., Zieger-Hofmann, M., & Stanek, K. P. (2024). Every intrusion has its time: New zircon U-Pb ages from the greater Antilles arc in the Cordillera central, Dominican Republic. *Lithos*, *486*, 107779.

Hastie, A. R. (2009). Is the Cretaceous primitive island arc series in the circum-Caribbean region geochemically analogous to the modern island arc tholeiite series? *Geological Society, London, Special Publications*, *328*(1), 399–409. https://doi.org/10.1144/SP328.16

Hatter, S. J., Palmer, M. R., Gernon, T. M., Taylor, R. N., Cole, P. D., Barfod, D. N., & Coussens, M. (2018). The evolution of the Silver Hills volcanic center, and revised ^{40}Ar/^{39}Ar geochronology of Montserrat, lesser Antilles, with implications for Island Arc volcanism. *Geochemistry, Geophysics, Geosystems*, *19*(2), 427–452. https://doi.org/10.1002/2017GC007053

Hawkesworth, C. J., & Powell, M. (1980). Magma genesis in the Lesser Antilles island arc. *Earth and Planetary Science Letters*, *51*(2), 297–308. https://doi.org/10.1016/0012-821X(80)90212-5

Hayden, L. A., Watson, E. B., & Wark, D. A. (2008). A thermobarometer for sphene (titanite). *Contributions to Mineralogy and Petrology*, *155*(4), 529–540. https://doi.org/10.1007/s00410-007-0256-y

Hu, H. Y., Stern, R. J., Rojas-Agramonte, Y., & Garcia-Casco, A. (2022). Review of geochronologic and geochemical data of the greater Antilles volcanic Arc and implications for the evolution of oceanic arcs. *Geochemistry, Geophysics, Geosystems*, *23*(4), e2021GC010148. https://doi.org/10.1029/2021GC010148

Iturralde-Vinent, M. A. (1998). Synopsis of the geological constitution of Cuba. *Acta Geologica Hispanica*, *33*(1–4), 9–56.

Iturralde-Vinent, M. A., Otero, C. D., García-Casco, A., & Van Hinsbergen, D. J. J. (2008). Paleogene Foredeep basin Deposits of north-Central Cuba: A record of arcarc-continent collision between the Caribbean and north American plates. *International Geology Review*, *50*(10), 863–884. https://doi.org/10.2747/0020-6814.50.10.863

Jackson, S. E., Pearson, N. J., Griffin, W. L., & Belousova, E. A. (2004). The application of laser ablation-inductively coupled plasma-mass spectrometry to in situ U–Pb zircon geochronology. *Chemical Geology*, *211*(1–2), 47–69. https://doi.org/10.1016/j.chemgeo.2004.06.017

Jochum, K. P., Nohl, U., Herwig, K., Lammel, E., Stoll, B., & Hofmann, A. W. (2005). GeoReM: A new geochemical database for reference materials and isotopic standards. *Geostandards and Geoanalytical Research*, *29*(3), 333–338. https://doi.org/10.1111/j.1751-908X.2005.tb00904.x

Jolly, W. T., & Lidiak, E. G. (2006). Role of crustal melting in petrogenesis of the Cretaceous Water island formation (Virgin Islands, northeast Antilles Island arc). *Geológica Acta*, *4*, 35–62.

Jolly, W. T., Lidiak, E. G., & Dickin, A. P. (2008). Bimodal volcanism in northeast Puerto Rico and the Virgin Islands (Greater Antilles Island Arc): Genetic links with Cretaceous subduction of the mid-Atlantic ridge Caribbean spur. *Lithos*, *103*(3–4), 393–414. https://doi.org/10.1016/j.lithos.2007.10.008

Jolly, W. T., Lidiak, E. G., Dickin, A. P., & Wu, T.-W. (1998). Geochemical diversity of Mesozoic island arc tectonic blocks in eastern Puerto Rico. In *Geological Society of America, special Paper 322(tectonics and Geochemistry of the northeastern Caribbean)* (pp. 67–98). https://doi.org/10.1130/0-8137-2322-1.1

Joyce, J. (1991). Blueschist metamorphism and deformation on the Samana Peninsula-A record of subduction and collision in the Greater Antilles. In P. Mann, G. Draper, & J. F. Lewis (Eds.), *Geologic and tectonic Development of the North America-Caribbean Plate boundary in Hispaniola* (pp. 47–76). Geological Society of America.

Kerr, A. C., Iturralde-Vinent, M. A., Saunders, A. D., Babbs, T. L., & Tarney, J. (1999). A new plate tectonic model of the Caribbean: Implications from a geochemical reconnaissance of Cuban Mesozoic volcanic rocks. *Geological Society of America Bulletin*, *111*(11), 1581. https://doi.org/10.1130/0016-7606(1999)111<1581:ANPTMO>2.3.CO;2

Kesler, S. E., & Sutter, J. F. (1979). Compositional evolution of intrusive rocks in the eastern Greater Antilles island arc. *Geology*, *7*(4), 197. https://doi.org/10.1130/0091-7613(1979)7<197:CEOIRI>2.0.CO;2

Labanieh, S., Chauvel, C., Germa, A., Quidelleur, X., & Lewin, E. (2010). Isotopic hyperbolas constrain sources and processes under the Lesser Antilles arc. *Earth and Planetary Science Letters*, *298*(1–2), 35–46. https://doi.org/10.1016/j.epsl.2010.07.018

Lapierre, H., Dupuis, V., Mercier De Lépinay, B., Bosch, D., Monié, P., Tardy, M., et al. (1999). Late Jurassic oceanic crust and Upper Cretaceous Caribbean plateau picritic basalts exposed in the Duarte igneous complex, Hispaniola. *The Journal of Geology*, *107*(2), 193–207. https://doi.org/10.1086/314341

Legendre, L., Philippon, M., Münch, P., Leticée, J. L., Noury, M., Maincent, G., et al. (2018). Trench bending initiation: Upper plate strain pattern and volcanism. Insights from the Lesser Antilles Arc, St. Barthelemy Island, French West Indies. *Tectonics*, *37*(9), 2777–2797. https://doi.org/10.1029/2017TC004921

Lindsay, J. M., Trumbull, R. B., & Siebel, W. (2005). Geochemistry and petrogenesis of late Pleistocene to recent volcanism in Southern Dominica, Lesser Antilles. *Journal of Volcanology and Geothermal Research*, *148*(3–4), 253–294. https://doi.org/10.1016/j.jvolgeores.2005.04.018

Longshore, J. D. (1965). *Chemical and mineralogical variations in the Virgin Islands batholith and its associated wall rocks [Ph.D. thesis]* (p. 94). Rice University.

Macdonald, R., Hawkesworth, C. J., & Heath, E. (2000). The Lesser Antilles volcanic chain: A study in arc magmatism. *Earth-Science Reviews*, *49*(1–4), 1–76. https://doi.org/10.1016/S0012-8252(99)00069-0

Manhes, G., Minster, J. F., & Allègre, C. J. (1978). Comparative uranium-thorium-lead and rubidium-strontium study of the Saint Sèverin amphoterite: Consequences for early solar system chronology. *Earth and Planetary Science Letters*, *39*(1), 14–24. https://doi.org/10.1016/0012-821X(78)90137-1

Marchesi, C., Garrido, C. J., Bosch, D., Proenza, J. A., Gervilla, F., Monié, P., & Rodriguez-Vega, A. (2007). Geochemistry of Cretaceous magmatism in eastern Cuba: Recycling of North American continental sediments and implications for subduction polarity in the Greater Antilles Paleo-arc. *Journal of Petrology*, *48*(9), 1813–1840. https://doi.org/10.1093/petrology/egm040

McCulloch, M. T., & Gamble, J. A. (1991). Geochemical and geodynamical constraints on subduction zone magmatism. *Earth and Planetary Science Letters*, *102*(3–4), 358–374. https://doi.org/10.1016/0012-821x(91)90029-h

McDonough, W. F., & Sun, S. (1995). The composition of the Earth. *Chemical Geology*, *120*, 223–253.

Middlemost, E. A. K. (1994). Naming materials in the magma/igneous rock system. *Earth-Science Reviews*, *37*(3–4), 215–224. https://doi.org/10.1016/0012-8252(94)90029-9

Montheil, L. (2023). *Évolution géodynamique du Nord-Est de la plaque Caraïbe depuis l'Eocène: Un nouveau regard sur la paléogéographie régionale [Ph.D. thesis]* (p. 304). Université de Montpellier.

Montheil, L., Philippon, M., Cornée, J.-J., BouDagher-Fadel, M., Van Hinsbergen, D. J. J., Camps, P., et al. (2023). Geological architecture and history of the Antigua volcano and carbonate platform: Was there an Oligo−Miocene lull in Lesser Antilles arc magmatism? *GSA Bulletin*. https://doi.org/10.1130/B36465.1

Montheil, L., Philippon, M., Münch, P., Camps, P., Vaes, B., Cornée, J., et al. (2023). Paleomagnetic rotations in the northeastern Caribbean region reveal major intraplate deformation since the Eocene. *Tectonics*, *42*(8), e2022TC007706. https://doi.org/10.1029/2022TC007706

Morel, M. L. A., Nebel, O., Nebel-Jacobsen, Y. J., Miller, J. S., & Vroon, P. Z. (2008). Hafnium isotope characterization of the GJ-1 zircon reference material by solution and laser-ablation MC-ICPMS. *Chemical Geology*, *255*(1–2), 231–235. https://doi.org/10.1016/j.chemgeo.2008.06.040

Müller, R. D., Seton, M., Zahirovic, S., Williams, S. E., Matthews, K. J., Wright, N. M., et al. (2016). Ocean basin evolution and global-scale plate reorganization events since Pangea breakup. *Annual Review of Earth and Planetary Sciences*, *44*(1), 107–138. https://doi.org/10.1146/annurev-earth-060115-012211

Mutch, E. J. F., Blundy, J. D., Tattitch, B. C., Cooper, F. J., & Brooker, R. A. (2016). An experimental study of amphibole stability in low-pressure granitic magmas and a revised Al-in-hornblende geobarometer. *Contributions to Mineralogy and Petrology*, *171*(10), 1–27. https://doi.org/10.1007/s00410-016-1298-9

Nagle, F., Stipp, J. J., & Fisher, D. E. (1976). K-Ar geochronology of the Limestone Caribbees and Martinique, Lesser Antilles, West Indies. *Earth and Planetary Science Letters*, *29*(2), 401–412. https://doi.org/10.1016/0012-821X(76)90145-X

Noury, M., Philippon, M., Cornée, J., Bernet, M., Bruguier, O., Montheil, L., et al. (2021). Evolution of a shallow volcanic arc pluton during arc migration: A tectono-thermal integrated study of the St. Martin Granodiorites (Northern Lesser Antilles). *Geochemistry, Geophysics, Geosystems*, *22*(12), e2020GC009627. https://doi.org/10.1029/2020GC009627

Pearce, N. J. G., Perkins, W. T., Westgate, J. A., Gorton, M. P., Jackson, S. E., Neal, C. R., & Chenery, S. P. (1997). A compilation of new and published major and trace element data for NIST SRM 610 and NIST SRM 612 glass reference materials. *Geostandards Newsletter*, *21*(1), 115–144. https://doi.org/10.1111/j.1751-908X.1997.tb00538.x

Philippon, M., & Corti, G. (2016). Obliquity along plate boundaries. *Tectonophysics*, *693*, 171–182. https://doi.org/10.1016/j.tecto.2016.05.033

Pin, C., Briot, D., Bassin, C., & Poitrasson, F. (1994). Concomitant separation of strontium and samarium-neodymium for isotopic analysis in silicate samples, based on specific extraction chromatography. *Analytica Chimica Acta*, *298*(2), 209–217. https://doi.org/10.1016/0003-2670(94)00274-6

Pindell, J., & Dewey, J. F. (1982). Permo-Triassic reconstruction of western Pangea and the evolution of the Gulf of Mexico/Caribbean region. *Tectonics*, *1*(2), 179–211. https://doi.org/10.1029/TC001i002p00179

Pindell, J. L., & Kennan, L. (2009). Tectonic evolution of the Gulf of Mexico, Caribbean and northern South America in the mantle reference frame: An update. *Geological Society, London, Special Publications*, *328*(1), 1–55. https://doi.org/10.1144/SP328.1

Plank, T. (2005). Constraints from Thorium/Lanthanum on sediment recycling at subduction zones and the evolution of the continents. *Journal of Petrology*, *46*(5), 921–944. https://doi.org/10.1093/petrology/egi005

Plank, T., & Langmuir, C. H. (1998). The chemical composition of subducting sediment and its consequences for the crust and mantle. *Chemical Geology*, *145*(3–4), 325–394. https://doi.org/10.1016/S0009-2541(97)00150-2

Plunder, A., Thieulot, C., & Van Hinsbergen, D. J. J. (2018). The effect of obliquity on temperature in subduction zones: Insights from 3-D numerical modeling. *Solid Earth*, *9*(3), 759–776. https://doi.org/10.5194/se-9-759-2018

Putirka, K. (2016). Amphibole thermometers and barometers for igneous systems and some implications for eruption mechanisms of felsic magmas at arc volcanoes. *American Mineralogist*, *101*(4), 841–858. https://doi.org/10.2138/am-2016-5506

Richard, P., Shimizu, N., & Allègre, C. J. (1976). ^{143}Nd/^{144}Nd, a natural tracer: An application to oceanic basalts. *Earth and Planetary Science Letters*, *31*(2), 269–278. https://doi.org/10.1016/0012-821X(76)90219-3

Rojas-Agramonte, Y., Williams, I. S., Arculus, R., Kröner, A., García-Casco, A., Lázaro, C., et al. (2017). Ancient xenocrystic zircon in young volcanic rocks of the southern Lesser Antilles island arc. *Lithos*, *290*, 228–252. https://doi.org/10.1016/j.lithos.2017.08.002

Román, Y. A., Pujols, E. J., Cavosie, A. J., & Stockli, D. F. (2021). Timing and magnitude of progressive exhumation and deformation associated with Eocene arc-continent collision in the NE Caribbean plate. *GSA Bulletin*, *133*(5–6), 1256–1266. https://doi.org/10.1130/B35715.1

Schrecengost, K. L. (2010). *Geochemistry and U/Pb zircon geochronology of the Virgin Islands batholith, British Virgin Islands [M.Sc. Thesis]* (p. 73). University of North Carolina.

Sláma, J., Košler, J., Condon, D. J., Crowley, J. L., Gerdes, A., Hanchar, J. M., et al. (2008). Plešovice zircon—A new natural reference material for U–Pb and Hf isotopic microanalysis. *Chemical Geology*, *249*(1–2), 1–35. https://doi.org/10.1016/j.chemgeo.2007.11.005

Smith, A. L., Schellekens, J. H., & Díaz, A.-L. M. (1998). Batholiths as markers of tectonic change in the northeastern Caribbean. In E. G. Lidiak & D. K. Larue (Eds.), *Tectonics and geochemistry of the northeastern Caribbean* (pp. 99–122). Geological Society of America. https://doi.org/10.1130/0-8137-2322-1.99

Spandler, C., Hammerli, J., Sha, P., Hilbert-Wolf, H., Hu, Y., Roberts, E., & Schmitz, M. (2016). MKED1: A new titanite standard for in situ analysis of Sm–Nd isotopes and U–Pb geochronology. *Chemical Geology*, *425*, 110–126. https://doi.org/10.1016/j.chemgeo.2016.01.002

Speed, R. C., Gerhard, L. C., & McKee, E. H. (1979). Ages of deposition, deformation, and intrusion of Cretaceous rocks, eastern St. Croix, Virgin Islands. *Geological Society of America Bulletin*, *90*(7), 629–632. https://doi.org/10.1130/0016-7606(1979)90<629:aoddai>2.0.co;2

Speed, R. C., Smith-Horowitz, P. L., Perch-Nielsen, K. S., Saunders, J. B., & Sanfilippo, A. B. (1993). Southern Lesser Antilles arc platform: Pre-late Miocene stratigraphy, structure, and tectonic evolution. In *Geological Society of America, Special Paper 277*.

Sun, S., & McDonough, W. F. (1989). Chemical and isotopic systematics of oceanic basalts: Implications for mantle composition and processes. *Geological Society, London, Special Publications*, *42*(1), 313–345. https://doi.org/10.1144/GSL.SP.1989.042.01.19

Tatsumi, Y., Hamilton, D. L., & Nesbitt, R. W. (1986). Chemical characteristics of fluid phase released from a subducted lithosphere and origin of arc magmas: Evidence from high-pressure experiments and natural rocks. *Journal of Volcanology and Geothermal Research*, *29*(1–4), 293–309. https://doi.org/10.1016/0377-0273(86)90049-1

Thomson, S. N., Gehrels, G. E., Ruiz, J., & Buchwaldt, R. (2012). Routine low-damage apatite U-Pb dating using laser ablation–multicollector–ICPMS. *Geochemistry, Geophysics, Geosystems*, *13*(2), 2011GC003928. https://doi.org/10.1029/2011GC003928

Toothill, J., Williams, C. A., Macdonald, R., Turner, S. P., Rogers, N. W., Hawkesworth, C. J., et al. (2007). A complex petrogenesis for an arc magmatic suite, St Kitts, Lesser Antilles. *Journal of Petrology*, *48*(1), 3–42. https://doi.org/10.1093/petrology/egl052

Torró, L., Cambeses, A., Rojas Agramonte, Y., Butjosa, L., Iturralde-Vinent, M., Lázaro, C., et al. (2020). Cryptic alkaline magmatism in the oceanic Caribbean arc (Camagüey area, Cuba). *Lithos*, *376*, 105736.

Torró, L., Proenza, J. A., Marchesi, C., Garcia-Casco, A., & Lewis, J. F. (2017). Petrogenesis of meta-volcanic rocks from the Maimón Formation (Dominican Republic): Geochemical record of the nascent Greater Antilles paleo-arc. *Lithos*, *278–281*, 255–273. https://doi.org/10.1016/j.lithos.2017.01.031

van Achterbergh, E., Ryan, C., & Griffin, W. L. (2001). *GLITTER user's manual: On-line interactive data reduction for the LA-ICP-MS microprobe* (Vol. 4).

van Hinsbergen, D. J. J., Iturralde-Vinent, M. A., Van Geffen, P. W. G., García-Casco, A., & Van Benthem, S. (2009). Structure of the accretionary prism, and the evolution of the Paleogene northern Caribbean subduction zone in the region of Camagüey, Cuba. *Journal of Structural Geology*, *31*(10), 1130–1144. https://doi.org/10.1016/j.jsg.2009.06.007

Verati, C., Patrier-Mas, P., Lardeaux, J. M., & Bouchot, V. (2014). Timing of geothermal activity in an active island-arc volcanic setting: First ^{40}Ar/^{39}Ar dating from Bouillante geothermal field (Guadeloupe, French West Indies). *Geological Society, London, Special Publications*, *378*(1), 285–295. https://doi.org/10.1144/SP378.19

Vermeesch, P. (2018). IsoplotR: A free and open toolbox for geochronology. *Geoscience Frontiers*, *9*(5), 1479–1493. https://doi.org/10.1016/j.gsf.2018.04.001

Vervoort, J. D., Plank, T., & Prytulak, J. (2011). The Hf–Nd isotopic composition of marine sediments. *Geochimica et Cosmochimica Acta*, *75*(20), 5903–5926. https://doi.org/10.1016/j.gca.2011.07.046

Vila, J. M., Andreieff, P., Bellon, H., & Mascle, A. (1986). Collage along an east-west transcurrent fault of ante Oligocene age in the northern Virgin-Islands (Antilles). *Comptes Rendus Geoscience*, *302*(3), 141–144.

Villa, I. M. (1998). Isotopic closure. *Terra Nova*, *10*(1), 42–47. https://doi.org/10.1046/j.1365-3121.1998.00156.x

Whetten, J. T. (1966). *Geology of St.Croix, U.S. Virgin islands* (pp. 177–240). Caribbean Geological Investigations. https://doi.org/10.1130/mem98-p177

White, W. M., Copeland, P., Gravatt, D. R., & Devine, J. D. (2017). Geochemistry and geochronology of Grenada and Union islands, Lesser Antilles: The case for mixing between two magma series generated from distinct sources. *Geosphere*, *13*(5), 1359–1391. https://doi.org/10.1130/GES01414.1

White, W. M., & Dupré, B. (1986). Sediment subduction and magma genesis in the Lesser Antilles: Isotopic and trace element constraints. *Journal of Geophysical Research*, *91*(B6), 5927. https://doi.org/10.1029/JB091iB06p05927

Wiedenbeck, M., Allé, P., Corfu, F., Griffin, W. L., Meier, M., Oberli, F., et al. (1995). Three natural zircon standards for U-Th-Pb, Lu-Hf, trace element and REE analyses. *Geostandards and Geoanalytical Research*, *19*(1), 1–23. https://doi.org/10.1111/j.1751-908X.1995.tb00147.x

10.1029/2024GC012057

Wilson, F. H., Orris, G., & Gray, F. (2019). Preliminary geologic map of the Greater Antilles and the Virgin Islands. In *US geological Survey Open-File report, 1039, pamphlet 50p, 2 sheets, scales 1:2,500,000 and 1:300,000*.

Workman, R. K., & Hart, S. R. (2005). Major and trace element composition of the depleted MORB mantle (DMM). *Earth and Planetary Science Letters*, *231*(1–2), 53–72. https://doi.org/10.1016/j.epsl.2004.12.005

Yavuz, F., & Döner, Z. (2017). WinAmptb: A Windows program for calcific amphibole thermobarometry. *Periodico di Mineralogia*, *86*(2), 135–167.

Zellmer, G. F., Hawkesworth, C. J., Sparks, R. S. J., Thomas, L. E., Harford, C. L., Brewer, T. S., & Loughlin, S. C. (2003). Geochemical evolution of the Soufriere Hills Volcano, Montserrat, Lesser Antilles Volcanic Arc. *Journal of Petrology*, *44*(8), 1349–1374. https://doi.org/10.1093/petrology/44.8.1349

References From the Supporting Information

Blichert-Toft, J., & Albarède, F. (1997). The Lu–Hf isotope geochemistry of chondrites and the evolution of the mantle–crust system. *Earth and Planetary Science Letters*, *148*(1–2), 243–258. https://doi.org/10.1016/s0012-821x(97)00040-x

Holland, T., & Blundy, J. (1994). Non-ideal interactions in calcic amphiboles and their bearing on amphibole-plagioclase thermometry. *Contributions to Mineralogy and Petrology*, *116*(4), 433–447. https://doi.org/10.1007/bf00310910

Jacobsen, S. B., & Wasserburg, G. J. (1980). Sm–Nd isotopic evolution of chondrites. *Earth and Planetary Science Letters*, *50*(1), 139–155. https://doi.org/10.1016/0012-821x(80)90125-9

Whitney, D. L., & Evans, B. W. (2010). Abbreviations for names of rock-forming minerals. *American Mineralogist*, *95*(1), 185–187. https://doi.org/10.2138/am.2010.3371